FLEXURAL TESTING OF MOLYBDENUM-SILICON-BORON ALLOYS REACTED FROM MOLYBDENUM, SILICON NITRIDE, AND BORON NITRIDE

A Thesis
Presented to
The Academic Faculty

By

Chris Rockett

In Partial Fulfillment
Of the Requirements for the Degree
Master of Science in Materials Science and Engineering

Georgia Institute of Technology

August 2007

Flexural Testing of Molybdenum-Silicon-Boron Alloys
Reacted from Molybdenum, Silicon Nitride, and Boron Nitride

Approved by:

Dr. Joe K. Cochran, Advisor
School of Materials Science and Engineering
Georgia Institute of Technology

Dr. Thomas H. Sanders, Jr.
School of Materials Science and Engineering
Georgia Institute of Technology

Dr. Naresh N. Thadhani
School of Materials Science and Engineering
Georgia Institute of Technology

Date Approved:

ACKNOWLEDGEMENTS

I would like to extend my gratitude to several people who have been instrumental in helping me complete this thesis. First and foremost to Dr. Cochran, whose faithful guidance and patience have brought me to this point; it was an honor to work under him. I am especially grateful to Michael Middlemas for showing me the ropes and for his constant assistance and advice during experimentation. I would also like to thank the committee members, Dr. Tom Sanders and Dr. Naresh Thadhani, who has been a faithful advisor since my undergraduate years at Georgia Tech.

TABLE OF CONTENTS

LIST OF TABLES

LIST OF FIGURES

SUMMARY

As a refractory metal with a melting temperature in excess of 2600°C, molybdenum shows promise as a candidate for the next generation jet turbine blade material. However, because of its catastrophic oxidation behavior, it must be protected with additional elements. Alloying molybdenum with silicon and boron improves its oxidation resistance via formation of a protective borosilicate glass surface scale.

In a novel processing route, silicon nitride and boron nitride powders are reactively sintered with high-purity molybdenum powder to form an alloy containing the intermetallic Mo_3Si and Mo_5SiB_2 phases dispersed in a matrix of Mo metal. This metal-matrix composite microstructure is thought to be ideal for both mechanical properties and oxidation resistance. This powder process uses commercially available raw materials and common industrial practices such as milling and spray drying which makes it amenable to commercial scale-up.

However, a persistent problem with Mo-Si-B alloys is their inherent brittleness at low temperature. While the powder processing method is shown to produce ductile pure Mo metal, it is evident that silicon in solid solution substantially raises the ductile-to-brittle transition temperature (DBTT) of the metal matrix. Because of this, even a small amount of room-temperature ductility has not been realized for Mo-Si-B alloys.

This project focuses on investigating the mechanical properties of Mo-Si-B alloys produced by the new processing route and the search for elemental additions or processing treatments that improve ductility. Alloying additions such as aluminum and tantalum are investigated and heat treatments are attempted. Mechanical properties are tested using four-point bending and phase compositions and microstructures characterized using x-ray diffraction and

scanning electron microscopy, respectively. It has become obvious through this research that the mechanical properties of Mo-Si-B alloys are almost entirely matrix controlled and that to enhance room temperature ductility, the solubility of silicon in molybdenum must be reduced or its detrimental effects somehow minimized.

CHAPTER 1

INTRODUCTION

Inside the combustion chamber of jet turbine engines is an exceptionally demanding environment for structural materials. Turbine blades must withstand temperatures above 1100°C[1] and centrifugal forces due to their high rotational velocity. Current nickel-based "superalloys", even with improved design, microstructural refinement, and elaborate cooling mechanisms, are reaching their maximum performance potential. But engine efficiency and specific power could be improved with elevated operating temperatures, so there is a need for new high-temperature structural materials. Molybdenum is a refractory metal with a melting point in excess of 2600°C and it possesses the necessary strength and creep resistance for turbine blade applications. However, its oxidation resistance is unacceptable, forming a non-adherent, volatile oxide around 750°C.

In the late 1990s it was realized that molybdenum silicides with boron additions may possess the necessary combination of mechanical properties and oxidation resistance for turbine blade applications. Mo-Si-B alloys form exceptionally thermally stable intermetallic phases and gain oxidation resistance via formation of a protective and adherent borosilicate scale on their surface. With a properly engineered microstructure, Mo-Si-B alloys could exhibit sufficient low- and high-temperature toughness and creep strength along with adequate oxidation resistance to supplant superalloys as a turbine blade material.

This research project focuses on alloys with the nominal composition Mo-3Si-1B (in wt%), whose microstructure consists of a mixture of α-Mo with Si and B in solid solution (Mo_{ss}), and the intermetallic phases Mo_3Si (A15) and Mo_5SiB_2 (T2). In order to achieve a satisfactory balance of mechanical and oxidative properties, the optimal microstructure is one of finely dispersed intermetallic phases in a continuous Mo_{ss} matrix. Most previous work[3, 7-11, 16] in the Mo-Si-B system has focused on melt processing or sintering of pre-alloyed powders. However, such methods can produce coarse microstructures, often containing non-equilibrium or thermally unstable phases, and create discontinuous Mo_{ss} dispersions.

A new processing route, reported on by Middlemas and Cochran[20] involves powder processing and reactive sintering of Mo-Si-B alloys using the nitrides of Si and B. Si_3N_4 and BN are stable precursors that will resist premature oxidation during storage and processing but then decompose to elemental Si and B during high-temperature sintering. This process has been proven to produce Mo-Si-B alloys of near theoretical density with fine-grained microstructures in the 1-4μm range. X-ray diffraction confirms the presence of the equilibrium Mo_{ss}, A15, and T2 phases while SEM micrographs reveal the optimal microstructure of a continuous metal matrix with dispersed intermetallics.[20]

The emphasis in this project is on determining strength and ductility for Mo-Si-B alloys produced by the nitride reactive sintering process. A range of compositions was tested and an experimental search for ductilizing additives and treatments to the Mo-Si-B system was conducted. Strength and ductility were assessed by flexural testing at room temperature and elevated temperatures.

This thesis begins with a review of the published literature on the development of Mo-Si-B alloys and their mechanical properties, as well as on ductility enhancement in molybdenum. Then an overview of the processing route will be given along with and explanation of selected materials, the compositional matrix, experimental procedures, and testing setup. In the results and discussion section the phase content and microstructures will be shown and then flexural testing data will be presented and related to compositional and processing variables. These microstructures and strength data will be compared to those in similar publications. Finally, conclusions will be drawn and recommendations for further studies will be made.

CHAPTER 2

LITERATURE REVIEW

In this section, literature pertinent to the mechanical properties of Mo-Si-B and molybdenum alloys is summarized. Particular emphasis is put on the ductility of molybdenum and of the Mo_{ss} matrix.

2.1 Foundational Work in the Mo-Si-B System

Molybdenum silicides, principally $MoSi_2$, exhibit superior oxidation resistance and have been used for decades as furnace heating elements.[2] The oxidation resistance of $MoSi_2$ is known to be the result the formation of a glassy silica layer on the surface of the molybdenum, which protects the underlying metal from rapid oxidation. However, $MoSi_2$ is much too brittle at room temperature and lacks sufficient creep strength to be used for high-temperature structural applications.

Other intermetallics in the Mo-Si system have been investigated as an alternative to $MoSi_2$; in particular, Mo_5Si_3 (the T1 phase) has been studied extensively. The creep resistance of T1 is higher than $MoSi_2$ due to the former's more complicated crystal structure, but its mid-temperature oxidation resistance is unacceptable (rapid oxidation up to 1650°C). Akinc et al.[3] investigated boron addition to the T1 phase and observed a five order of magnitude improvement in oxidation resistance between 800° and 1500°C.

Working on the foundation laid by Nowotny et al.[4] who developed the Mo-Si-B ternary phase diagram (see Figure 1), Berczik[5] discovered that silicon and boron added in small amounts (i.e. 1-4wt% each) drastically improve the oxidation resistance of molybdenum while still retaining its favorable high-temperature strength. This is attributed to the formation of a protective borosilicate glass layer whose wetting capability is enhanced by boron. Berczik was granted patents on Mo-Si-B alloys that may be described as composites with a metal matrix and discrete intermetallic dispersions. This microstructure is ideal for affording oxidation resistance while preserving the mechanical properties of the base metal.

Berczik's alloys lie within the compatibility triangle bounded by the Mo(Si,B) solid solution (Mo_{ss}) and the intermetallic phases Mo_3Si (A15) and Mo_5SiB_2 (T2). Berczik has concentrated on alloys with a nominal composition of Mo-3Si-1B in wt% (Mo-8.9Si-7.8B in at%).

Akinc and colleagues have focused on Mo-Si-B alloys containing A15, T2, and Mo_5Si_3 (T1) phases. Although these alloys exhibit exceptional oxidation resistance and are promising candidates for improved furnace elements, in absence of a Mo matrix they inherently lack the ductility necessary for turbine blade applications.

Sluggish kinetics and slow diffusion rates in the Mo-Si-B system are responsible for its high-temperature phase stability. However, this aspect makes microstructural modification via heat treatment or other means impractical for Mo-Si-B, unlike most structural alloys. Perepezko[6] likens these alloys to ceramics and composites in that the initial synthesis methods determine the

final microstructure. For these reasons, a processing route that produces a suitable final microstructure is important.

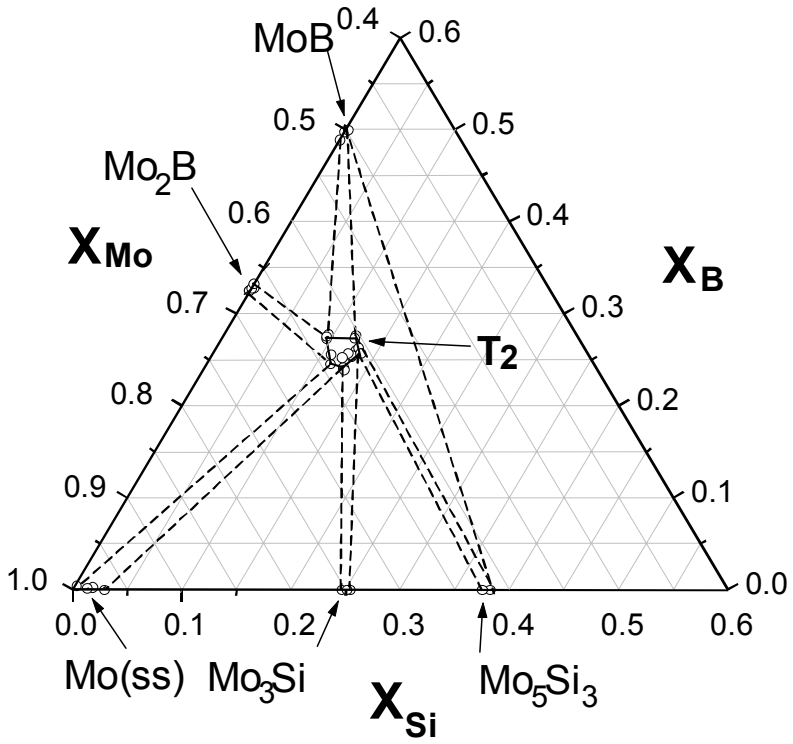

Fig. 1: Isothermal section (1600°C) of the molybdenum-rich portion of the Mo-Si-B phase diagram, [4]

Several other research groups are investigating Mo_{ss}-A15-T2 alloys and processing routes, oxidation resistance, and mechanical properties thereof. Schneibel et al.[7] have studied a wide range of compositions from 7-20at% Si and 0-18at% B. Specimens were tested in three-point flexure at room temperature and the results are summarized in Table 1. It was noted that compositions containing around 25vol% Mo (actually Mo_{ss}, but these terms will be used interchangeably throughout) exhibited macroscopic cracking upon casting. The data suggest that increased Mo content brings about a rise in strength. Strength also appears to rise with increasing B content, although this is qualitatively attributed to a finer microstructure.

In other studies, Choe and Schneibel[8,9] demonstrated the effect of the Mo matrix and its microstructure on fracture toughness at ambient and elevated temperatures. In the first report[8] they essentially confirmed the benefit of a continuous Mo matrix produced via a powder metallurgy route. This microstructure ensures that a propagating crack cannot avoid the ductile toughening phase, and the coarser microstructure is known to improve ductile phase toughening mechanisms. In the latter, more recent study[9], they employed two different processing methods: ingot metallurgy (IM) via arc-melting, casting and annealing; and powder metallurgy (PM) via hot isostatic pressing (HIPing) of pulverized arc castings. Powder metallurgy was done to circumvent the problem of cracking that inevitably occurs when casting with high Si content. The microstructures of these samples consisted of Mo particles distributed throughout a network of the intermetallic phases A15 and T2. A representative micrograph is shown in Figure 2. Despite this non-ideal microstructure, toughness improvements were observed due to two principle toughening mechanisms: crack trapping at low temperatures and ductile-phase bridging at elevated temperatures. In summary, they saw superior toughness for the IM samples due to their higher Mo volume fraction and coarser microstructure. The PM processed samples lacked such toughness because of their low Mo content and finer microstructure.

Table 1: Room temperature flexural strength data for Schneibel et al. compositions and phase volume fraction (%) estimates, [7]

Composition (at.%)	α-Mo volume fraction (%)	Strength (MPa, as-cast)	α-Mo	Mo_3Si	T2
Mo–7Si–12B		597	53.1	4.1	42.8
Mo–10Si–7B	≈50	431	49.5	26.2	24.3
Mo–12Si–6B		470	43.0	36.2	20.8
Mo–12Si		322	49.5	50.5	
			28.0	4.4	67.6
Mo–10Si–18B		303	26.7	37.4	35.9
Mo–14Si–10B	≈25	463	25.8	60.3	13.9
Mo–20Si		18	21.1	78.9	

Alur and Kumar et al.[21] have studied compressive behavior of Mo-Si-B alloys at temperatures between 1000-1400°C. Through compression testing of a two-phase (Mo_{ss} + T2) Mo-6.1Si-7.9B and a three-phase (Mo_{ss} + A15 + T2) Mo-8.6Si-8.7B (at%) they determined that deformation is matrix controlled. This was concluded because of significant overlap in the response of the two- and three-phase materials to the strain rates and temperatures evaluated. A commercially available Mo-Ti-Zr (TZM) alloy was also tested for baseline comparison. Their alloys were produced by plasma rotating electrode processing (PREP) and exhibited only a somewhat continuous molybdenum matrix with a 37% volume fraction of T2. They observed silica lamellae alternating with the T2 phase as well as at some T2/Mo_{ss} interfaces, however it is not suspected that this substantially affects flow behavior because it is co-mingled with T2 and does not appear to provide preferential crack paths.

Hardness measurements on the Mo_{ss} matrix made apparent that significant solid-solution strengthening as well as work-hardening contribute to the much higher flow stress of the Mo-Si-B compositions over TZM. Alur and Kumar proposed a third mechanism that can contribute to

the strength and deformation behavior, a geometric effect often observed in discontinuously reinforced composites. Rigid reinforcement particles (intermetallic dispersions in this case) impose constraints on the deformation of the matrix, causing triaxial stresses to develop.

In absence of other published literature on the Mo-(Si,B) solid solution Jain, Alur, and Kumar[22] performed compression tests on the Mo_{ss} matrix material. This was prepared as a Mo-0.75Si-0.14B (wt%) alloy containing approximately 3-5vol% of the T2 phase using arc melting. This solid solution alloy was split into two samples: one subjected to extrusion and the other to isothermal forging. Another two-phase Mo-2Si-1B (wt%) was made using powders prepared by PREP and consolidated by HIPing. Pure molybdenum was also tested for comparison. Similar to the previous study, compression tests were conducted in a vacuum over the temperature range of 1000-1200°C and at strain rates from 10^{-7} to 10^{-4} s^{-1}. The potent solid-solution strengthening effect of Si is seen in the 3x higher flow stress of the solid solution alloy samples as compared to pure Mo. Not only are the solid solution and two-phase alloys stronger, but they exhibit appreciable work hardening unlike pure Mo. This is especially evident for the two-phase alloy, in which the aforementioned geometric constraint effect is present.

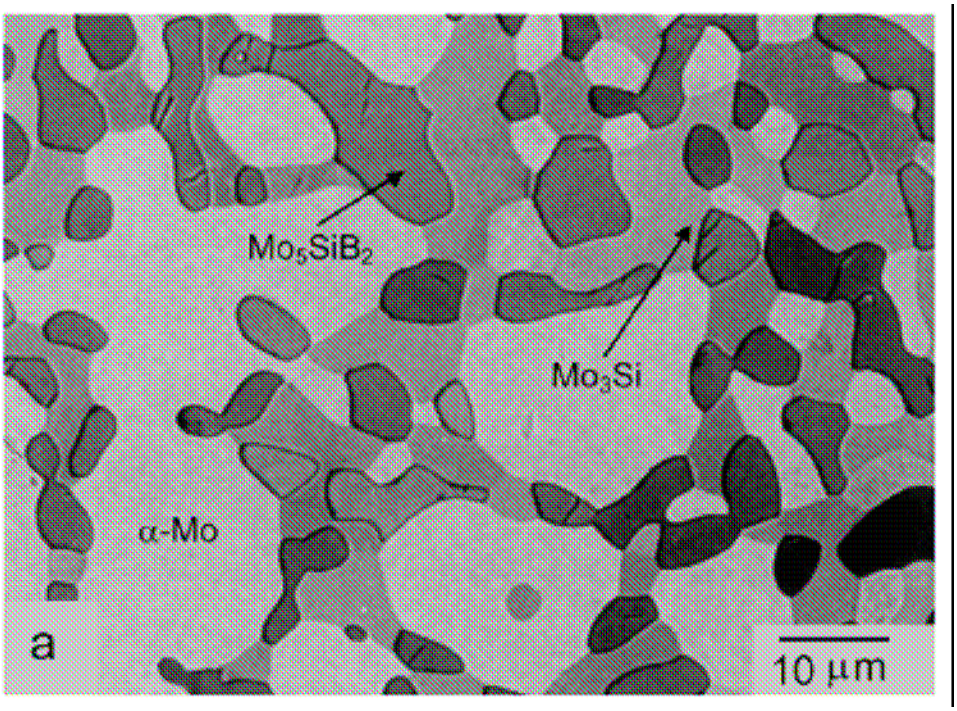

Fig. 2: Micrograph of Choe and Schneibel's IM processed alloy with discrete Mo particles, [9]

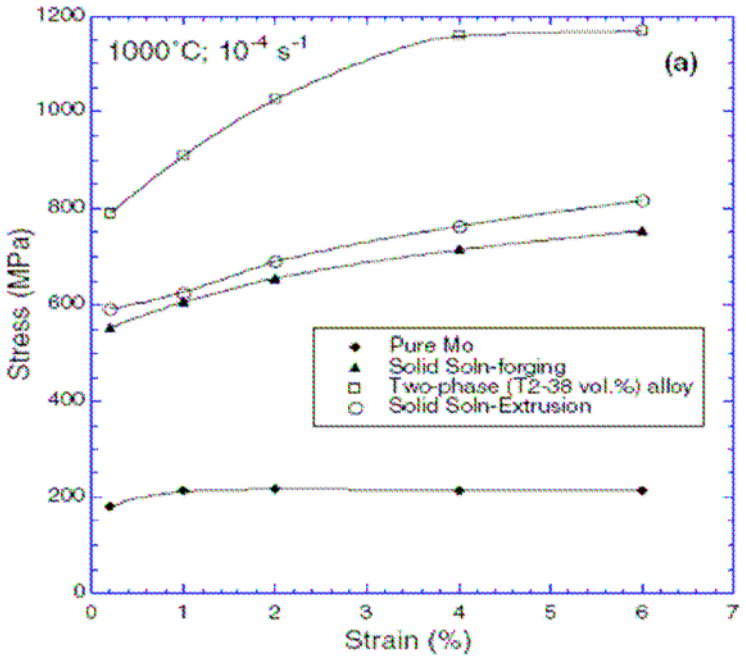

Fig. 3: Compressive stress-strain response at 1000°C for the solid solution alloy, two-phase alloy, and pure Mo, [22]

Jéhanno and a group at Plansee AG[10] have produced and characterized alloys of the composition Mo-8.9Si-7.7B (at%) (Mo-3Si-1B in wt%, hereafter referred to as "3/1") using their usual industrial PM method and tested their high-temperature mechanical properties. Through refinement of the x-ray diffraction pattern, they arrived at phase volumes of 55% Mo_{ss}, 15% A15 and 30% T2 with an overall theoretical density (T.D.) of 9.62 g/cm^3. The ductile-to-brittle transition temperature (DBTT) was determined from 3-point bending tests in vacuum at 1000-1200°C, observing ductile behavior above ~1100°C and brittle behavior below. They also stressed the potential benefits of a microstructure consisting of a Mo_{ss} matrix with dispersed intermetallic particles. Indeed, after extrusion (6:1 reduction ratio) of a HIPed 3/1 alloy, the evolution of the microstructure to one in which dispersed intermetallic particles are surrounded by a Mo_{ss} matrix saw a dramatic increase in ductility and tensile strength (see Figures 4 and 5).[11] Note the 200°C drop in DBTT realized by the extrusion.

The research reported in all of the aforementioned studies makes it clear that, for turbine blade applications, Mo-Si-B alloys must strike a compromise between mechanical properties on one hand, and oxidation resistance on the other. An alloy of nearly pure Mo will exhibit superior ductility and creep resistance, but will lack any oxidation resistance. An entirely intermetallic alloy may exhibit fantastic oxidation resistance, but will lack acceptable ductility for use in turbine engines. It has, however, been discussed that ductilization of the Mo_{ss} matrix itself could allow for higher fractions of oxidation-resistant intermetallics while still retaining the favorable mechanical properties of the Mo matrix. To this end, many studies have focused on ductilization of molybdenum and its alloys.

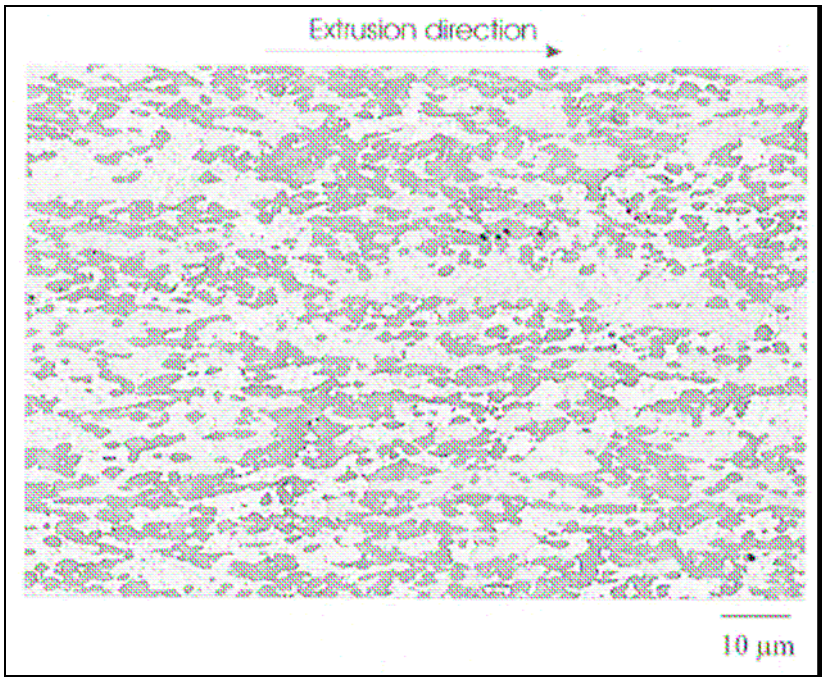

Fig. 4: Microstructure obtained by the Jéhanno and the Plansee group after extrusion of a 3/1 composition. The light phase is Mo_{ss} and the darker phases are A15 and T2, [11]

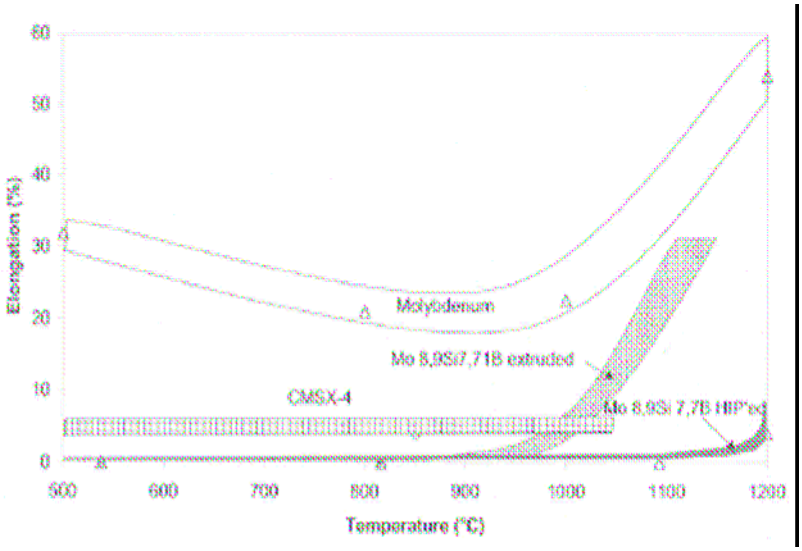

Fig. 5: Ductility comparison of Plansee's Mo-Si-B alloy before and after extrusion with a commercial single crystalline superalloy (CMSX-4) and pure Mo, [11]

2.2 Molybdenum Ductility

Olds and Rengstorff[12,13] have reported on the effects of impurities and alloying elements on the ductility of cast molybdenum. Most commercially available molybdenum exhibits brittleness in the as-cast state unless its grain structure is refined via heat treatment. However, the authors did observe ductility in coarse-grained, as-cast molybdenum when it was sufficiently pure.

These and several other studies report the ductile-to-brittle transition temperature as an indication of room-temperature ductility. Molybdenum and other metals of the body-centered cubic structure exhibit a change from ductile to brittle behavior as the test temperature is lowered. The lower its DBTT, the more ductile a specimen is considered. Olds and Rengstorff performed bending tests and used a threshold bend angle at failure to define the onset of embrittlement.

In their first study, the effects of oxygen, nitrogen, and carbon impurities were determined quantitatively. It was found that oxygen was the most harmful impurity – a mere 0.0002% (2 p.p.m.) saw a rise in DBTT from -60 to 200°C. Nitrogen and carbon were much less detrimental: embrittlement occurred at 0.003% N_2 and 0.014% C.

Their subsequent study was on the effects of alloying elements on ductility. They reasoned that strong oxide, nitride, and carbide formers ought to reduce the detrimental effects of the aforementioned impurities. Ti, Th, Al, Ce, V, B, and Zr additions were chosen and they found these to fall into three categories: 1) those which have an optimal value (i.e. a minimum in DBTT) in the curve of transition temperature vs. composition (Ti, Ce, B, V); 2) those which have no optimal value and cause an increase in brittleness (i.e. increase in DBTT with increasing alloy

content: Zr, Al); and 3) those which have no optimal value and cause a decrease in brittleness with increasing alloy content (Th).

It is relevant to the present investigation that boron fell into the first category. A minimum in DBTT was observed at .005% B (it is not expressed in the paper whether these are weight or atomic percentages, but the latter seems to have been the convention in metallurgical publications of the 1950s) and further additions raised the DBTT in a roughly parabolic fashion. They speculated that boron neutralizes the harmful effects of oxygen by forming strong oxides. However, the level of boron addition required to do this is extremely small and boron levels in a 3/1 composition are in excess of 0.005%. Probably for additions above this level the normal solid solution hardening effect takes over, increasing strength at the cost of ductility.

It is also thought that Al should scavenge excess oxygen from the molybdenum, possibly improving ductility. However, Olds and Rengstorff found that Al fell into category 2 so any level of addition increased the DBTT. Titanium imparted the greatest improvement in ductility and accomplished this over the largest compositional range.

In addition to impurities and alloying elements, processing conditions play a role in the ductility of molybdenum. Suzuki et al.[14] investigated the effect of post-processing heat treatment on the ductility of arc-melted molybdenum, also employing a bend test to determine DBTT. They observed a significant drop (~100°C) in DBTT with annealing at 700°C for 12 hours under a H_2 atmosphere. But for other specimens of ultra-high purity, the drop in DBTT was not seen, leading them to conclude that the benefit from annealing must result from a change in the state of

interstitial impurities (substitutional impurities are not mobile enough at these temperatures to cause an appreciable effect). It is thought that the annealing effect is due to carbon segregating at grain boundaries, which either 1) reacts with other embrittling impurities and makes them ineffective, or 2) increases grain boundary cohesion. Moreover, removal of interstitial carbon from the matrix may reduce the solid solution hardening effect, thereby softening the matrix and enhancing ductility. This would also mean that only regions of the matrix adjacent to grain boundaries would be softened, relaxing the stress concentrations that would otherwise lead to intergranular fracture.

As a final note on carbon impurities in molybdenum, it is worth mentioning the thorough study of grain boundary segregation of carbon by Kumar and Eyre.[15] Through auger electron spectroscopic analysis of fracture surfaces, they confirmed that oxygen segregation to grain boundaries is a major cause of brittleness in Mo alloys and that carbon segregation may improve ductility. It does so by three proposed methods: 1) gettering of oxygen, thereby reducing O segregation to grain boundaries, 2) Mo_2C precipitates at grain boundaries act as dislocation sources, and 3) these precipitates form semi-coherent interfaces between adjacent grains, thereby reducing grain boundary energy.

2.3 Alloying Additions to the Mo-Si-B System

Working on the principle of improving the ductility of the Mo matrix in Mo-Si-B alloys Schneibel et al.[16] considered three alloying additions. Zirconium was chosen based on the properties of TZM alloys (Mo-0.5Ti-0.1Zr in wt%) because it is known to getter interstitials such as C and O. A maximum in fracture toughness was observed around 2.0at% Zr, although the

mechanism involved is unknown. Spinel ($MgAl_2O_4$) particles were also investigated based on previous successes with ductility improvement in chromium.[17] A preliminary experiment confirmed that ductility is enhanced in powder processed Mo by 9vol% spinel additions, as compared to pure molybdenum. However, the investigation left many questions unanswered such as what were the minimum and maximum beneficial amounts and whether the same effect could be observed in a Mo-Si-B intermetallic alloy. Finally, in light of the well established improvement of Mo ductility by rhenium[18], Schneibel suggests further investigation into Mo-Re-Si-B system to determine, among other factors, how Re would partition into the intermetallic phases and whether these would remain stable. However, the higher density of Mo-Si-B alloys versus current superalloys is already a concern because of increased engine weight and centrifugal forces and addition of an extremely high-density element such as Re (21 g/cm^3) will only worsen this problem.

Aluminum additions to Mo-Si-B were investigated by Mitra et al.[19] They prepared a Mo-12Si-8B-3Al (in at%), a Mo-11.2Si-8.1B-7.2Al, and a Mo-14B-10B alloy for comparison. Prior to hot pressing, the aluminum-containing powders were held at 700°C for 1 hr in order to allow molten aluminum to react with SiO_2 and form Al_2O_3 particles. This reaction is expected based on the lower free energy of formation of aluminum oxide versus that of silica. Chemical analysis of the Mo-Si-B (sans aluminum) microstructures revealed that dark areas which appear to be pores are actually pockets of glassy silica, existing in an amount near 9vol%. Microstructures of the aluminum-containing samples reveal around 10vol% alumina particles and increased A15 content. This is attributed to extra free Si liberated by Al scavenging oxygen from silica. In this manner, the A15 phase is increased at the expense of Mo matrix. Calculations reveal that 1.6at%

and 6.2at% Al will be available for alloying in the 3%Al and 7.2%Al compositions, respectively. It is also known that some fraction of the Al will go into solid solution with either the Mo matrix or A15, creating a substituted A15 phase, $Mo_3(Si_{1-x}Al_x)$, where x is found to be .24 and .36 in the 3%Al and 7.2%Al compositions, respectively. The 3%Al specimens exhibited fracture strengths around 340 MPa compared to 170 MPa for the 7.2%Al specimens. This reduced flexural strength is more likely the result of the non-uniform distribution and lower volume fraction of the Mo matrix rather than alloying effects of Al.

Currently, the investigation of mechanical properties Mo-Si-B alloys is focused primarily on observing and understanding fundamental fatigue, creep, and crack growth mechanisms. These investigations are important for lifetime predictions and design guidelines. On the other hand, publications on ductilization of the Mo matrix have been sparse. In light of the groundwork done in this area, more investigations into alloying additions and heat treatments are needed. Conspicuously lacking is a thorough, systematic study of Si and B dissolution in molybdenum and the resulting effect on ductility.

CHAPTER 3

EXPERIMENTAL PROCEDURES

In this chapter the techniques used to prepare, characterize, and test samples are discussed. A powder processing method similar to that used for ceramics is employed using the nitride precursors as aforementioned. High purity raw materials are blended into powder, pressed, and densified to create samples for characterization and mechanical testing. Characterization was done using scanning electron microscopy (SEM) and x-ray diffraction (XRD). Attempts at ductilizing the Mo_{ss} matrix were made, including alloying additions and heat treatments. Testing was done at room temperature and elevated temperatures to observe any possible changes in DBTT.

3.1 Nitride-based Powder Processing and Reactive Sintering

The powder metallurgical route has proven to produce the desired Mo-Si-B microstructures. Fine powders ensure a fine grain structure and homogeneity. However, fine powders of Si and B will oxidize readily in air. These oxides are very stable and correspondingly difficult to reduce, thus they would be carried into the final microstructure. Silica in the microstructure is particularly detrimental to high temperature strength, being a weak, glassy inclusion. Accordingly, raw materials were sought that would be protected from oxidation during storage and processing.

The nitrides of Si and B are very stable up to about 1000°C given their high low-temperature Gibbs free energies of formation, but readily decompose to elemental Si and B at sintering temperatures (see Figure 6).

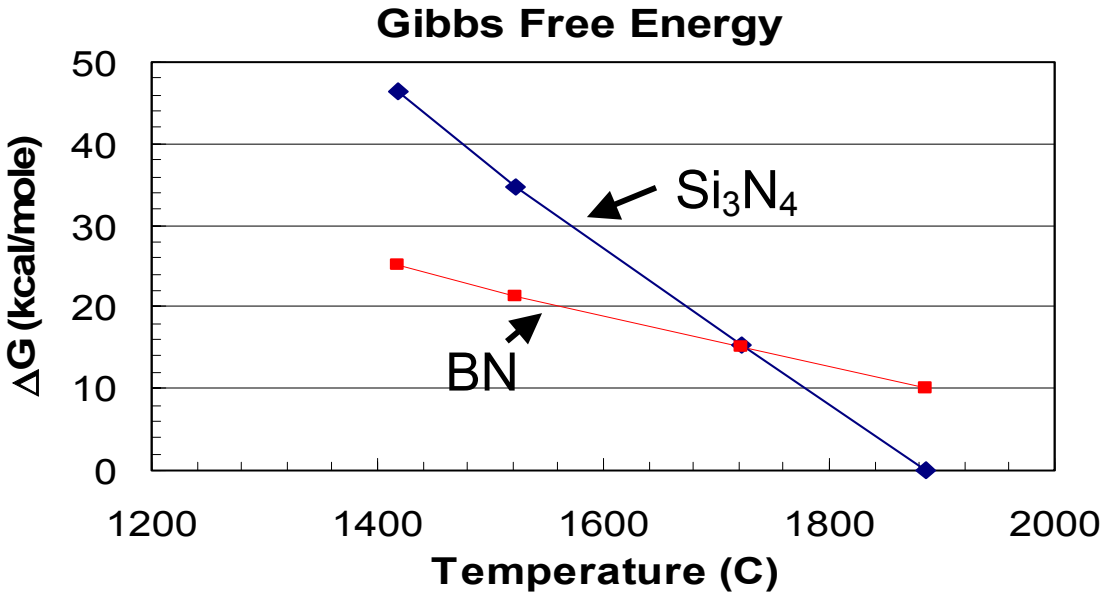

Fig. 6: High temperature free energies of the silicon and boron nitrides, [20]

There are several proposed reactions for the decomposition of the nitrides and formation of the intermetallic phases. Middlemas[20] has shown via XRD that the formation of A15 and T2 begins around 1300°C and is complete by 1400°C. This confirms that the Mo is reacting directly with the nitrides and assisting in their decomposition, likely according to the following reactions:

$$\text{A15:} \quad 3\,Mo + 1/3\,Si_3N_4 \rightarrow Mo_3Si + 2/3\,N_2 \qquad (1)$$

$$\text{T2:} \quad 2Mo + Mo_3Si + 2BN \rightarrow Mo_5SiB_2 + N_2 \qquad (2)$$

3.2 Raw Materials

Sub-micron sized powders were chosen to enhance sintering and facilitate decomposition of the nitrides. Table 2 gives a summary of the properties of the Mo-Si-B raw materials. The first compositions prepared and tested had a constant 3:1 silicon to boron ratio with an increasing volume fraction of the Mo_{ss} matrix, between 56 and 75vol%. Also prepared were various solid solution compositions with just enough Si and/or B to see minimal formation of intermetallic phases. In this manner, the properties of the matrix material alone could be observed.

Other alloying additions were investigated in this project. Aluminum was chosen with hopes to improve oxidation resistance via formation of mullite. Two aluminum compositions were prepared: one as a solid solution, and the other with 70vol% Mo and intermetallic phases. In both cases, the Al to Si ratio was 3:1. For these compositions, 99.9% pure, 1-5µm sized Al powder was used (Atlantic Equipment Engineers). Tantalum was chosen in the hope that it may improve ductility in the Mo-Si-B alloys, either because of its own inherent ductility or because its reactivity could pull Si out of solid solution in molybdenum. Tantalum powder (99.8% pure, 1-5µm, Atlantic Equipment Engineers) was used for two compositions: a pure, baseline alloy of Mo with 6wt% Ta and a Mo-(Ta,Si) solid solution.

Table 2: Specifications and properties of Mo-Si-B raw materials, adapted from [20]

Molybdenum	**Grade**	**Purity**	**Particle Size**	**Surface Area (m^2/g)**	**Oxygen Content**
Climax	Ultrafine	99.95%	100-500 nm	3.3	0.8 wt%
Silicon Nitride	**Grade**	**Purity**	**Particle Size**	**Surface Area (m^2/g)**	**Oxygen Content**
UBE Industries	SN-E03	99%	~0.5 μm	4	0.82 wt%
Boron Nitride	**Grade**	**Purity**	**Particle Size**	**Surface Area (m^2/g)**	**Oxygen Content**
Cerac	B-1084	99.50%	0.73 μm	6.7	N/A

3.3 Powder Preparation

In order to ensure homogeneous distribution of the constituents, the raw powders are dissolved in acetone, milled, and spray dried. These processing steps will be described in detail in this section.

The slurries consist of the raw powders dissolved with a binder/dispersant and a lubricant in acetone. Poly(methyl methacrylate) (PMMA 2008, Ineos Acrylics) is added up to 1wt% as a binder and also functions as a dispersant to keep the powders suspended and prevent agglomeration via formation of a monolayer on particle surfaces. Stearic acid is added up to 0.5wt% as a lubricant to aid in subsequent dry pressing. These organics are dissolved in acetone and ball milled in polyethylene jars overnight before the addition of the Mo, Si_3N_4, and BN powders. As an example, for a 3/1 composition, the necessary proportions of starting materials were determined by stoichiometric calculations of the decomposition reactions to be 92.94wt%

Mo, 4.84wt% Si_3N_4 and 2.22wt% BN. The powder slurry is then energetically milled in a paint shaker for 60 minutes prior to spray drying. Middlemas[20] has shown the microstructural benefits of energetic milling and spray drying.

Spray drying is a process that produces granules from solutions or suspensions by atomizing them into a chamber in which drying air is being circulated. The process has been used for many years, in industries ranging from food to technical ceramics, to produce quality powders inexpensively and with high yields. Spray drying ensures thorough dispersion of powder mixtures and a predictable, even distribution of spherical granule sizes. Spherical granules facilitate deformation and flow during dry pressing of powders, which leads to higher pressed or "green" densities.

The Mo-Si-B slurries were dried using the Büchi 190 Mini Spray Dryer (Brinkmann Instruments) depicted in Figure 7. This machine consists chiefly of a spray nozzle, fluid pump, aspirator motor, drying chamber, and collection traps. A suspension or solution of the desired solid in a suitable solvent (known as a slurry) is pumped via a peristaltic pump into the spray nozzle (3). Here, the slurry is mixed with compressed air (or some other chosen gas) and atomized into the primary drying chamber, at the bottom of which is a coarse collection trap into which larger particles fall. The drying air (1), which may be heated (2), is supplied by the aspirator motor and will carry finer powder particles into the conical cyclone chamber (4). Here, the fine powder will dry fully and make its way into the fine collection trap (8), while dust and solvent vapors are drawn out the top and vented (5).

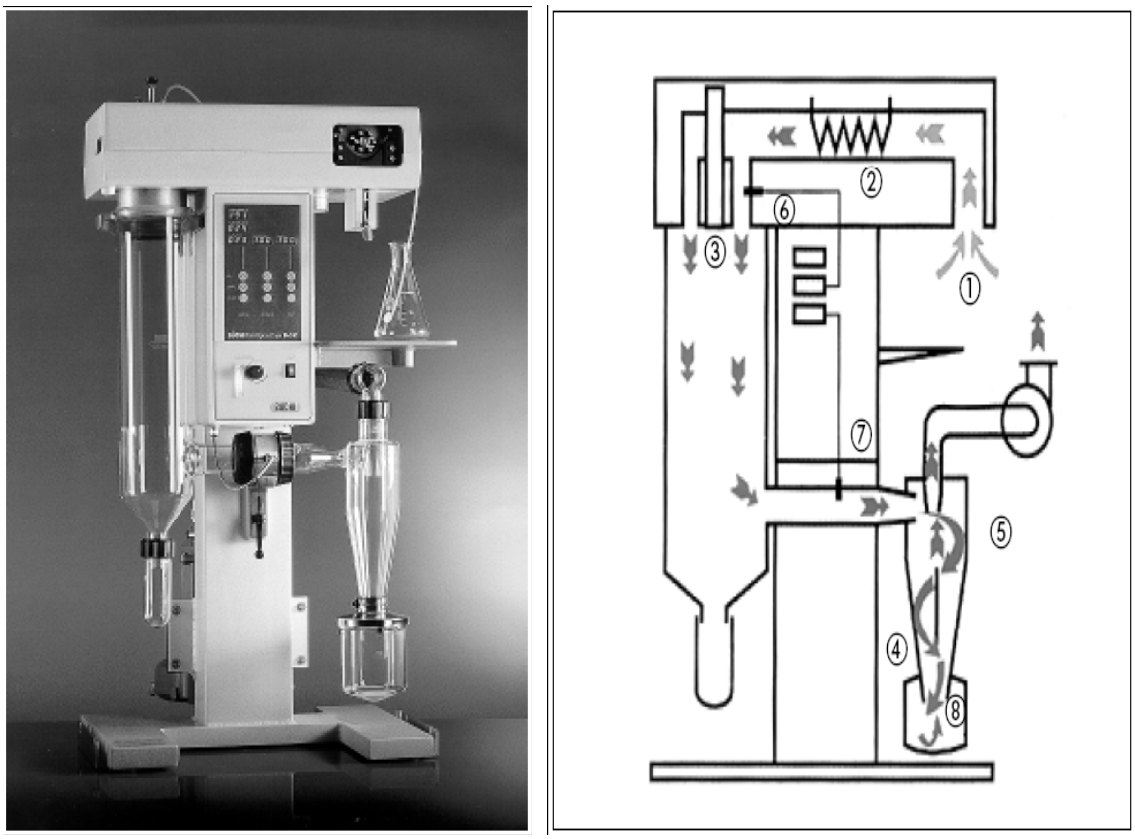

Fig. 7: Photograph and schematic of Büchi 190 Mini Spray Dryer, courtesy of Büchi training papers

Spray drying is optimized by controlling machine parameters as well as adjusting slurry properties. Slurry properties include solids content, solvent choice, and additions of binders and dispersants, all of which affect its viscosity and flow behavior, as well as final powder properties. The spray dryer itself offers control over several parameters including fluid pump (feed) rate, compressed air flow rate, aspirator rate, and drying air temperature. All of these have an appreciable effect on the properties of the finished powder as well as yields.

Through initial experimentation with the spray dryer it was quickly determined that 15vol% was the maximum solids loading that could be fed through the spray nozzle. Machine parameters were tweaked and the resultant powder observed in order to produce spherical powder particles

in the desired size range. As a final step, the powder is screened to sub-140 mesh (106µm) to remove large agglomerates and impurities. The following is a micrograph of some representative spray-dried Mo-Si-B powder. The compositions prepared and tested in this project are listed in table 3.

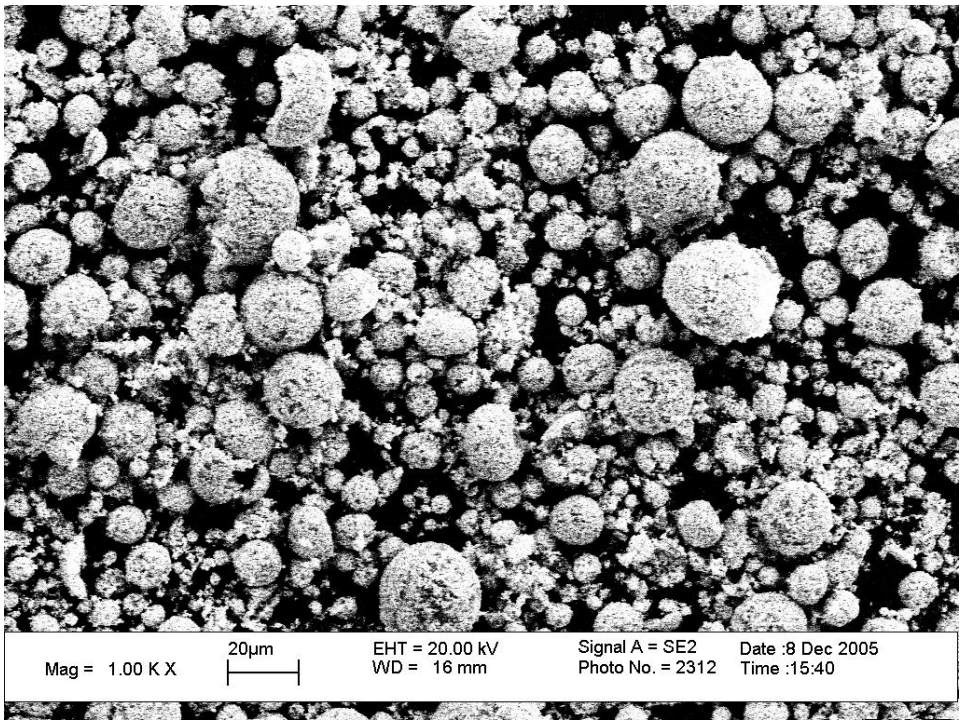

Fig. 8: SEM micrograph of spray dried Mo-Si-B powder

Table 3: Compositions prepared and tested in this project

Composition	wt% Mo	wt% Si	wt% B	wt% Other	at% Mo	at% Si	at% B	vol% Mo_{ss}	vol% T2	vol% A15
56Mo-3/1	96.00	3.00	1.00	-	83.46	8.87	7.68	56.97	27.09	15.94
60Mo-3/1	96.25	2.81	0.94	-	84.37	8.37	7.26	60.06	25.48	14.46
65Mo-3/1	96.65	2.51	0.84	-	85.86	7.58	6.56	64.99	22.87	12.14
70Mo-3/1	97.05	2.21	0.74	-	87.38	6.76	5.86	69.96	20.28	9.76
75Mo-3/1	97.45	1.91	0.64	-	88.94	5.93	5.14	75.00	17.64	7.36
Mo-(Al,Si,B) S.S.	95.88	1.00	0.12	3.0wt% Al	86.4	3.1	0.01	85.0	1.8	13.2*
70Mo-(Al,Si,B)	94.95	1.10	0.65	3.3wt% Al	82.0	3.3	5.0	63.4	17.4	18.7*
Mo-0.67%Si S.S.	99.33	0.67	-	-	97.70	2.30	-	99.19	-	0.81
Mo-1.1%Si S.S.	98.90	1.10	-	-	96.36	3.64	-	93.34	-	6.66
Mo-(Si,B) S.S.	99.24	0.73	0.035	-	97.26	2.43	0.30	98.00	1.00	1.00
Mo-6%Ta	93.60	-	-	6.4wt% Ta	96.50	-	-	100.00	-	-
Mo-(Ta,Si) S.S.	92.70	1.00	-	6.3wt% Ta	93.20	3.43	-	94.71	-	5.29**

* Estimated assuming formation of Mo_3Al A15 analog

** Not certain due to lack of Mo-Ta-Si phase diagram

3.4 Dry Pressing

Dry pressing is the uniaxial compression of powders into a mold cavity (die). For this project the dies available were a ½-inch diameter cylindrical die and a 1" x 0.1" rectangular die (see Figure 9). These were used to produce, respectively, ½-inch diameter pellets and one-inch bars roughly $1/10^{th}$-inch square in cross section (before firing). Pellets are used for SEM observation and XRD characterization and bars are used as flexural test specimens.

Pressing was done with an electrically actuated hydraulic press (Carver Inc.) to ensure a steady rise to pressure. Early pressing experiments by Middlemas[20] produced the green density curve in Figure 10 and showed that 70ksi is an optimal pressure which produces green compacts of about 54% theoretical density (TD). It was also shown conclusively that spray dried powder is superior for dry pressing, evident both in the green state and the final microstructure.

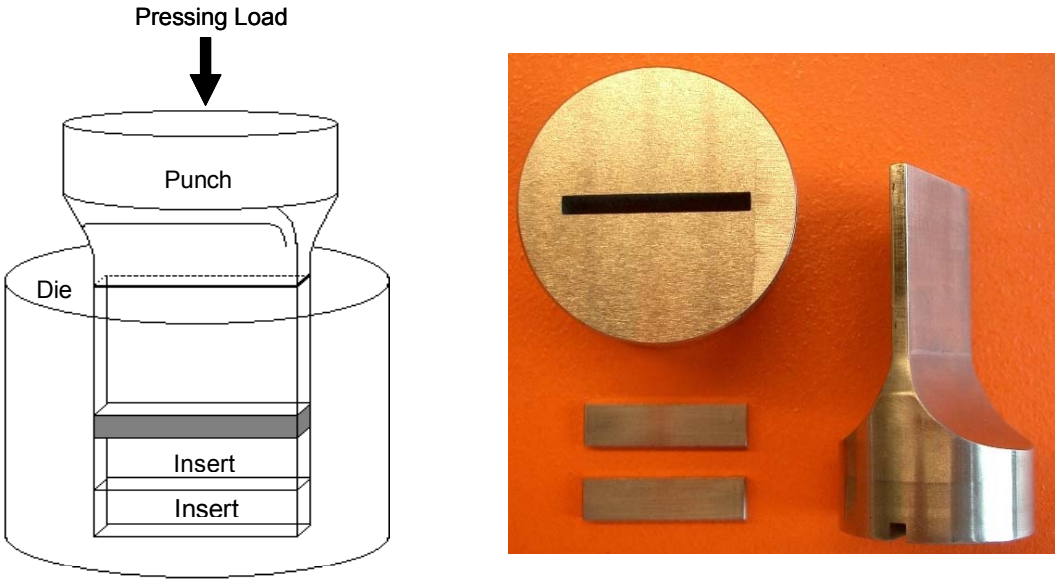

Fig. 9: Schematic and photograph of rectangular die and punch set

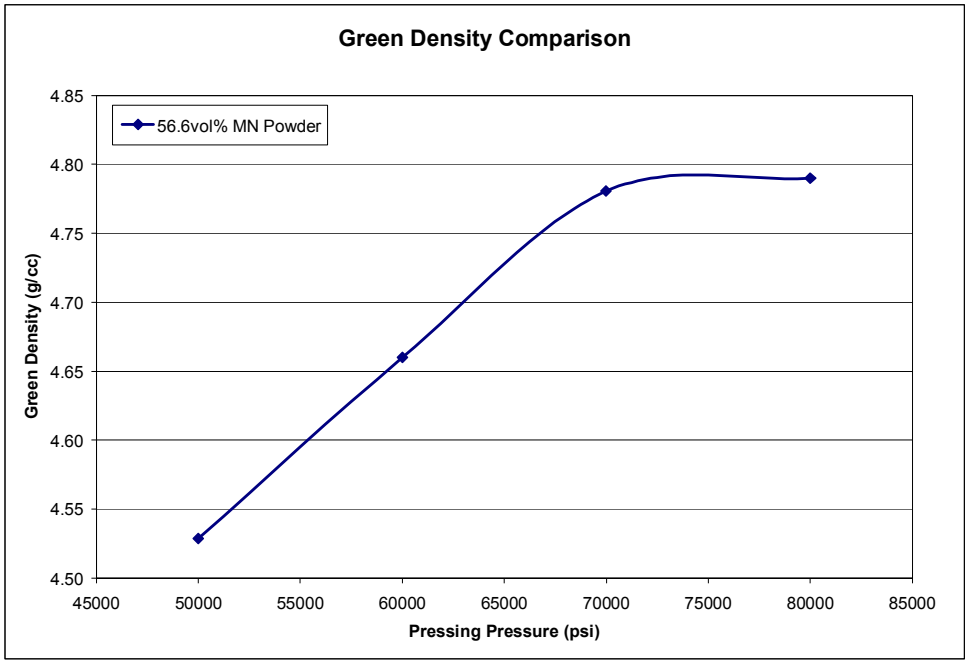

Fig. 10: Relationship between pressing pressure and resultant green density, [20]

3.5 Binder Removal

In the early stages of the project, XRD phase identification indicated that molybdenum carbide (Mo_2C) was forming during firing, presumably from the organic binder and lubricant in the powder mixture. The original furnace setup employed by Middlemas had many fittings and consequently many opportunities for air leaks. Oxidation occurring during firing was apparent in that a ~100μm skin, depleted in intermetallic content, was forming at the surface of the pellets. After an overhaul of the furnace tube and gas routing, a much cleaner, controlled atmosphere was realized inside the furnace. This eliminated the problem of skin formation but had a side effect: apparently the air leaks had been sufficient to oxidize and remove the carbon within the samples, but in their absence, Mo_2C was able to form. Another factor that may have hindered binder removal was the switch from 3/8"-diameter pellets to 1/2" pellets, which create a longer path for carbon to escape from the center to the edge of a pellet.

Several methods were attempted to remove the binder in the green compact before firing in order to avoid carbide formation. One was to soak the samples in acetone overnight to leach out the binders. The soak-out technique appeared to work, as weight changes in the samples corresponded with binder weights. However, this left the samples distended and weakened, adversely affecting sintering. Another method is to program a two-hour hold at 300°C into the furnace schedule to allow sufficient time for binder burnout in the inert atmosphere. A third method is to simply bake the green samples in air at 200°C for 12 hours. Without a doubt, this removes organics, but significant oxidation effects have been

observed. In light of these issues, a systematic study of binder removal was carried out and will be reported in the results section of this thesis.

3.6 Sintering

Sintering is a densification process in which green bodies are fired at high temperatures sufficient to promote diffusion. Because of their high surface areas, small powder particles will tend to coalesce in order to reduce surface energy. In this manner, a green compact will densify to a solid body with near theoretical density (the density of a specimen with zero porosity). In the nitride-based processing method, reactive sintering occurs, during which the boron and silicon nitrides react with molybdenum and decompose, forming the intermetallic phases. Samples were placed in high-purity alumina boats (McDanel) and fired in a 24" tube furnace (MHI) with a 3/4" diameter alumina tube (Vesuvius). The firing atmosphere consists of 10%H_2 with a balance of Ar and total gas flow is around 60cc per minute. Hydrogen is a reducing agent and will react with oxygen from the atmosphere and reduce MoO_3 (but not B_2O_3 or SiO_2). Additional efforts are taken to avoid oxygen in the firing atmosphere. The furnace tube is pumped down to vacuum and back-filled with the Ar/H_2 mixture three times before starting the furnace schedule. A gettering furnace filled with titanium sponge operating at 750°C is also placed upstream to scavenge any oxygen impurities in the atmosphere.

Sintering studies performed by Middlemas[20] showed that the intermetallic formation was complete by 1400°C, but fired density increased dramatically with further increases

in temperature. Being the maximum practical temperature achievable in the available furnaces, 1600°C was established as the sintering temperature. A hold time of six hours at this temperature was determined to be sufficient. The intermetallic grains coarsen between two and six hours but no change was observed for a hold time of twelve hours.

3.7 Characterization

Several characterization methods were used to identify the phases present, measure physical properties, and observe the microstructures of the samples produced. These include x-ray diffraction (XRD), scanning electron microscopy (SEM), and density measurements.

3.7.1 X-Ray Diffaction

XRD analysis was performed using a Philips PW1800 diffractometer using Cu-Kα radiation. Samples were first ground to the center and polished flat to avoid misleading readings from the surface due to oxidation or other contamination. Phase identification was done using Philips X'Pert HighScore Plus software. For XRD scans displayed throughout, intensity has been normalized to the highest Mo (110) peak to highlight smaller peaks.

3.7.2 Density Measurements

The density of pellets and bar specimens was determined using two methods. Standard geometrical density is calculated by dividing mass by volume measurements made with a

micrometer. This method has the potential for error due to specimen irregularities such as warping, cupping, bubbling or chipping, but gives sufficient qualitative comparison ability.

A more accurate measurement of density is the Archimedes method which involves finding the weights of a specimen when dry, saturated, and suspended in water. Bulk density is determined by the following equation:

$$\rho_{Bulk} = \frac{W_{Dry}}{W_{Sat} - W_{Susp}} \ , \tag{3}$$

where W_{Dry} is dry weight, W_{Sat} is the weight when saturated with water, and W_{Susp} is the weight when both saturated and suspended in water. Before such measurements, the samples are boiled in water for 30 minutes to ensure full saturation of all open pores on the surface.

3.7.3 Scanning Electron Microscopy

Microstructures were examined in a Leo 1530 or 1550 SEM with a backscatter detector (BS-SEM). Backscatter mode creates phase contrast based on the atomic weights of the phase constituents. For this reason, Mo will show up lighter and the intermetallic phases darker. Pellets were ground to the center to ensure a cross section representative of the bulk material (this also allows for examination of edges to compare with the bulk). The A15 and T2 phases are indistinguishable due to their similar average atomic weights. Porosity appears black as do SiO_2 inclusions, which can be difficult to distinguish.

The Leo microscope is also equipped with an energy dispersive spectroscopic (EDS) analyzer (Oxford Instruments) and INCA analysis software. This allows for detection of elements and their relative abundance, although this information should be interpreted only as a qualitative assessment. EDS affords the capability to distinguish SiO_2 from voids, but EDS detects boron only poorly, still confounding the ability to distinguish one intermetallic phase from another.

3.8 Flexural Testing

Flexural testing was chosen because of the limited specimen geometries available via dry pressing. Three- and four-point bending are the most common methods for testing brittle materials such as ceramics because they eliminate the problem of specimen gripping and can be performed on as-received specimens without further forging or machining. Four-point bending is the preferred configuration because three-point bending exposes only a small fraction of the length of the specimen to the maximal stress state and tends to overestimate fracture stress.

Testing was performed on an *Insight 2* universal tester (MTS Systems Corp.) with an environmental chamber (Thermcraft Inc.) using a custom built four-point bending fixture. The thermal chamber is capable of a maximum safe temperature of 200°C. Unfortunately, this is not likely high enough to observe a ductile transition in the Mo-Si-B alloys, but it does open the possibility of observing a change in DBTT if it could be reduced

significantly. Unless otherwise indicated, all testing was done at 200°C. Figure 11 is a depiction of the test setup and fixture.

Bending was done at crosshead speeds between 0.15 and 1.00 mm/min, corresponding to approximate strain rates of 9.0E-5 and 6.0E-4 s^{-1}, respectively, according to the equation given in the ASTM standard method.[23] Load (in N) and crosshead displacement (in mm) were recorded. Fracture stress was computed with the following equation:

$$\sigma = 3PL_1 / 4tc^2, \quad (4)$$

where P is the load at failure, L_1 is the length from the bottom support to the first upper load point (1/3 of the lower span in this case), t is the width, and c is half the specimen height.

For any stress-strain curves given, strain has been calculated by

$$\varepsilon = 6dh / [(L_2-L_1)(L_2+2L_1)], \quad (5)$$

where d is the crosshead displacement, h is specimen height, L_2 is the lower span length, and L_1 is the upper span length (1/3 of the lower span in this case).

The *Insight 2* is designed primarily for precision testing of polymers and other comparatively weak specimens. Under the high loads involved with Mo-Si-B alloys, the test machine and fixture undergo significant deflection, which manifests as false strain. By running a test on a much thicker bar, whose stiffness is quasi-infinite relative to the test specimens, a compliance curve is generated that represents only the deformation that occurs in the test apparatus itself. This curve is fitted with a polynomial equation and this

equation may be applied to later bend testing results in order to subtract out the displacement due to machine and fixture compliance.

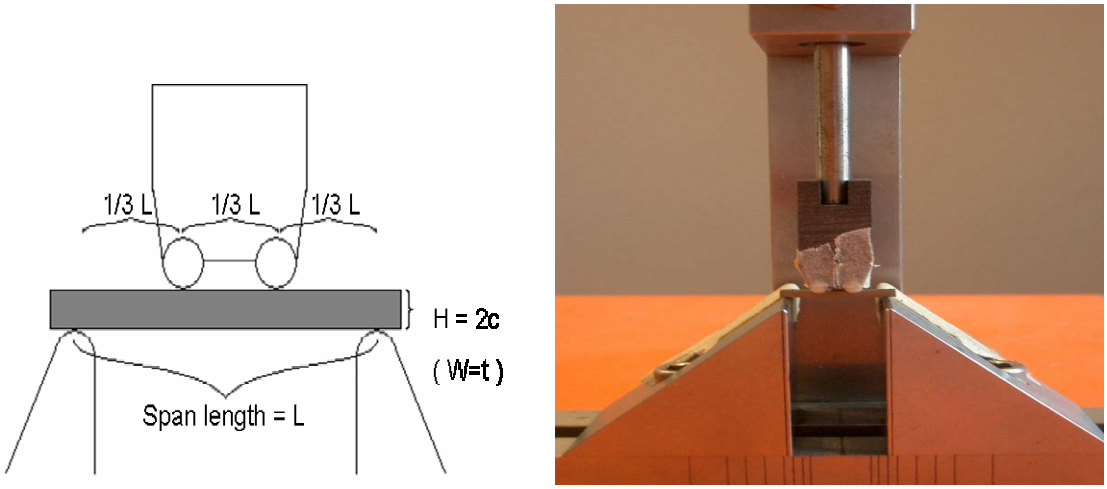

Fig. 11: Schematic and photograph of four-point bending test setup and fixture

CHAPTER 4

RESULTS AND DISCUSSION

In this section, the results of preparation, characterization, and testing of the Mo-Si-B alloys are discussed. Different processing conditions such as binder burnout methods were explored and their effects will be reported. Phase composition and microstructures were observed and will be explained. Flexural testing results are presented and attempts will be made to correlate these data to microstructural, compositional, and processing variables.

4.1 Pure Molybdenum Samples

Initial attempts at pressing Climax molybdenum powder produced poor results. The raw powder did not press well so the compacts would break apart upon ejection from the die. Thus the pure Mo powder was spray dried with binder and lubricant. This improved pressing drastically and produced pristine fired samples of an average density of 10.02 g/cm^3 or around 98% T.D.

Flexural testing of these pure Mo specimens revealed substantial ductility – up to 19% strain. The stress strain curves and a picture of the deformed specimen are shown in Figure 12. Exceptionally high strengths were also observed for these specimens: 1100 MPa on average compared to published values of ultimate tensile strength at 515 MPa.[24] These high strengths may be explained by the strong grain size dependence of Mo

according to the Hall-Petch relationship (an average grain size of 7μm is seen in Figure 13).

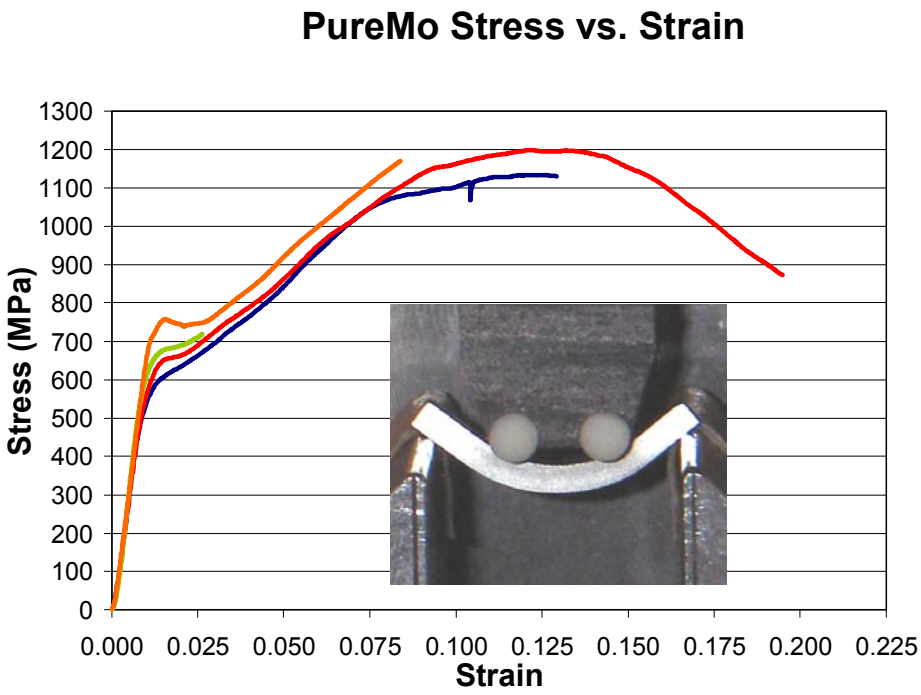

Fig.12: Stress/strain curve for pure Mo specimens and photo of ductile behavior

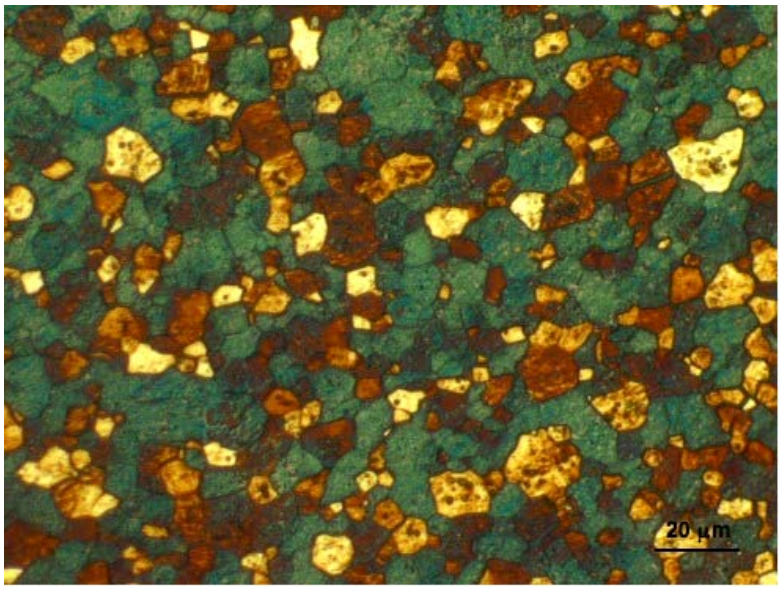

Fig. 13: Optical micrograph of pure Mo specimen (artificial color for enhanced contrast), average grain size is 7μm. Courtesy of P. Jain and K.S. Kumar.

These results validate that the processing method is sound and does not degrade the properties of the metal. Oxygen is often cited as the impurity most detrimental to ductility (see literature review section). Although powder metallurgy gives many opportunities for oxygen contamination, it is apparent that firing in hydrogen is sufficient to reduce MoO_3 and remove most of the embrittling oxygen. Because this processing route can produce ductile molybdenum, it should not be the cause of brittleness observed in other Mo-Si-B specimens, but rather solid solution and dispersion hardening effects.

4.2 Mo-Si-B Compositions

The next step in the project focused on observing the effects of Mo_{ss} matrix content on strength and ductility. To study this, a range of compositions between 56 and 75vol% Mo were prepared. Samples prepared from these powders fired to an average density around 92% of theoretical. The effects of densities on the mechanical behavior of Mo-Si-B specimens will be discussed in a later section.

The microstructures of each of these compositions are shown in Figure 14, and a close-up shot of the 56Mo-3/1 pellet is shown in Figure 15. Grain size is in the 1-4µm range. Note the similarity between these and the microstructure by Jéhanno et al. in Figure 5. Since the continuous Mo matrix and well-dispersed intermetallic phases are present in the as-fired condition, the nitride-based powder metallurgy method is quite attractive and viable for producing Mo-Si-B alloys suitable for turbine blades.

Some load vs. displacement curves are shown in Figure 16. These have not been corrected for compliance, so the displacement is not indicative of true strain in the samples. Accordingly, the slope of any of these curves should not be interpreted as an accurate elastic modulus for the samples. The bend tests merely give an indication of brittle behavior by their constant linear slope until failure, as opposed to ductile behavior indicated by a deviation from linearity. Fracture strengths may be compared qualitatively between specimens and compositions, but should not be interpreted as an accurate yield strength value. Immediately it is apparent that all of the compositions failed in a brittle manner. Mo_{ss} volume fraction thus had no effect on ductility and very little on strength.

Table 4: Density data for Mo-Si-B compositional range

Composition (vol% Mo)	Avg. Density (g/cc)	%T.D.
56	8.7237	91.44
60	8.8619	92.50
65	8.9789	93.14
70	8.9125	91.98
75	8.7482	89.72

It was expected that a 75vol% metal matrix would necessarily impart some ductility in the alloys, but this effect was not seen. It became apparent, then, that the matrix itself is brittle and unable to impart any low temperature ductility. In light of this, a 0.674wt% Mo solid solution was prepared in order to investigate the mechanical properties of the pure matrix material. At this level of Si addition, only a small fraction (<1vol%) of the A15 intermetallic forms, while the Mo metal is fully saturated with respect to Si. Initial testing of these samples revealed brittle behavior similar to any of the more heavily

alloyed specimens. This confirms the potent solid solution strengthening effect of silicon on molybdenum, even in the absence of hard intermetallic inclusions. The presence of such intermetallic inclusions probably explains the higher fracture strengths of the 56-75vol% Mo-3/1 samples versus the Mo-(Si) S.S. ones.

Another solid solution composition was prepared, this time with 0.73wt% Si and 0.035wt% B, enough to saturate the matrix with both of these constituents. Its behavior was unremarkably similar to that of the Si-only solid solution (see Figure 16). This suggests that B has little hardening effect on the alloys compared with Si, at least at low temperatures. It is suspected, however, that an interstitial solute such as B may impart resistance to deformation at high temperatures. Densities for the solid solution compositions averaged about 9.6 g/cm^3 or about 96% T.D.

Annealing was attempted to determine its effect on strength and ductility. It was thought that an annealing cycle might affect the solubility of Si in Mo. Mo_{ss} specimens were annealed for 12hrs at 700°C in a pure H_2 atmosphere. No improvement in ductility was seen, but annealing apparently brought about a 50 MPa increase in average fracture strength (see Figure 21). Although these specimens were tested at different strain rates (0.15 or 0.50 mm/min), this did not produce an observable effect on their behavior.

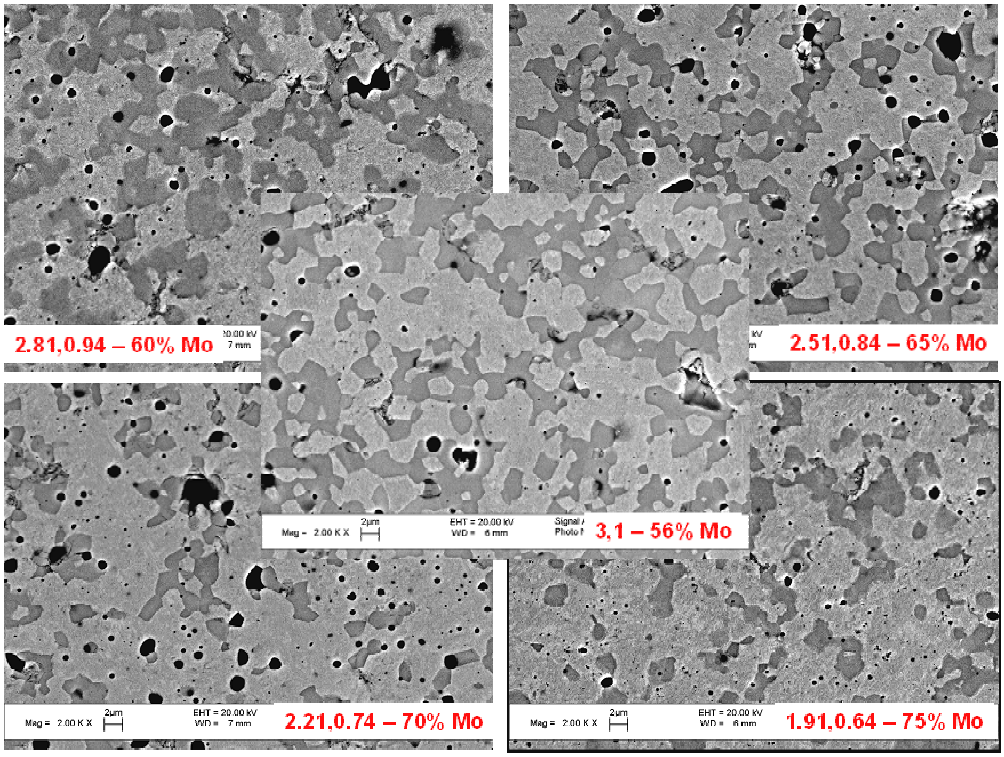

Fig. 14: SEM micrographs of a range of compositions between 56 and 75vol% Mo matrix

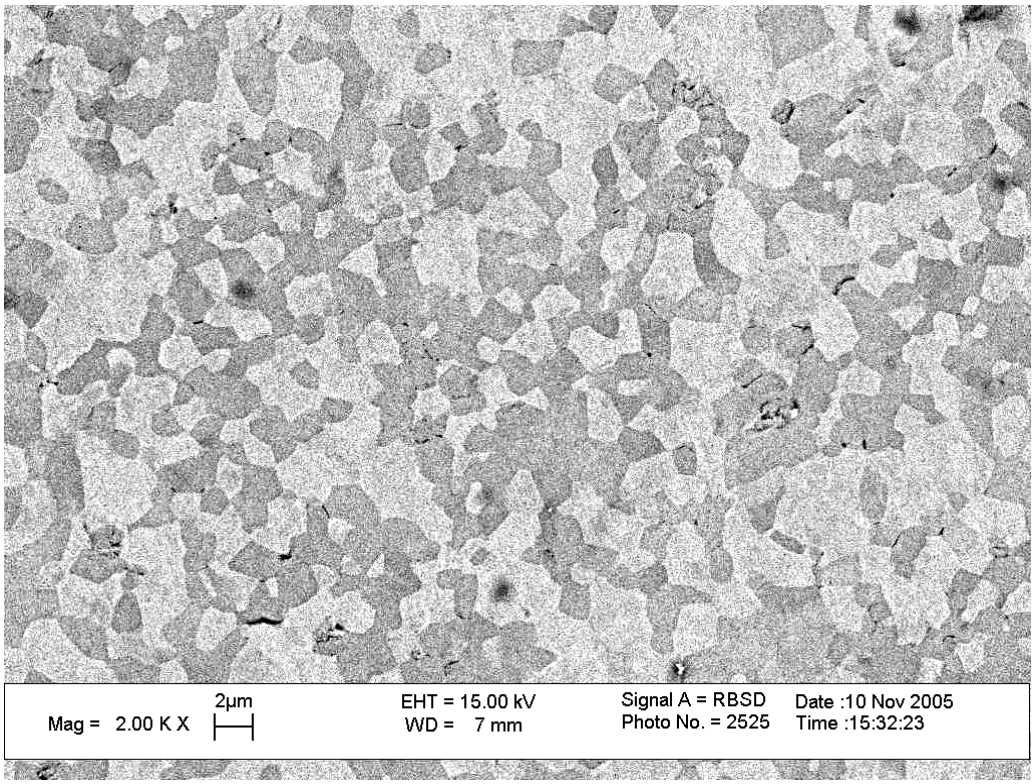

Fig. 15: SEM micrograph of 56Mo-3/1 microstructure

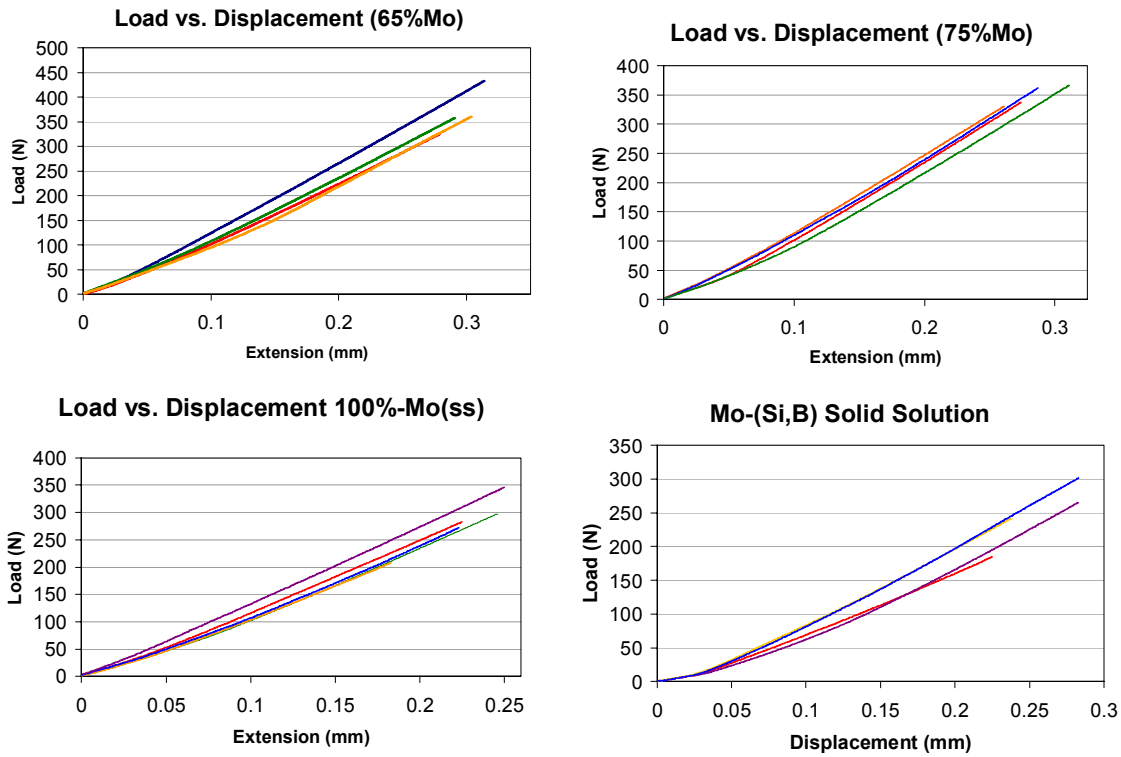

Fig. 16: Load vs. displacement curves for Mo-Si-B alloys, compositions as noted

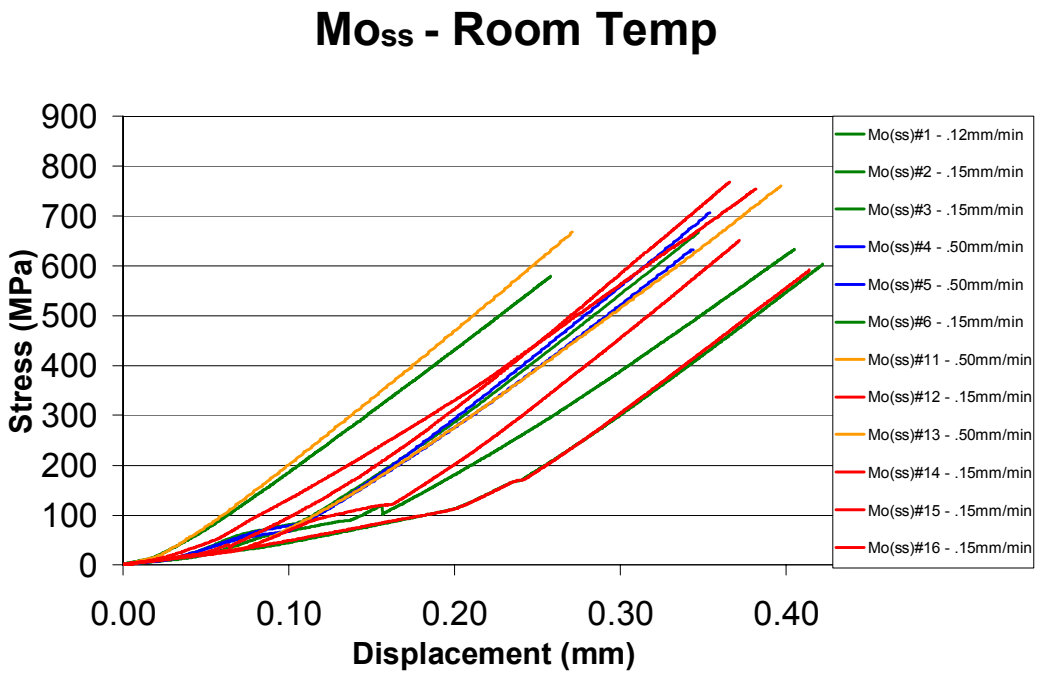

Fig. 17: Stress vs. displacement curves for Mo_{ss} specimens tested at two different strain rates and annealing treatments. Specimens numbered 1-6 were as-fired, 11-16 were annealed at 700°C in H_2 for 12 hours after firing.

4.3 Porosity Issues

Porosity is inherent to powder processing. Powder characteristics such as size distribution, flocculation, and particle geometry will affect green density, which will in turn affect sintering ability. Most of the alloys prepared in this project fired to average densities of about 93% of theoretical (the density value for a specimen with zero porosity). As mentioned in the previous section on SEM characterization, pores (voids) are visibly indistinguishable from silica inclusions, and since silica is comparatively light weight, its presence would cause a reduction in density comparable to voids. Accordingly, it is expected that these silica inclusions would also adversely affect strength and other mechanical properties in much the same way as voids.

The failure of brittle materials in bending is a probabilistic phenomenon. Failure occurs when a critically sized flaw nucleates a crack which can then propagate rapidly through the material. Strengths obtained from bending will always have a spread in value, often as much as 25%. In light of this, the next step in the project was to determine the effect of porosity on flexural behavior.

Densities were measured for the samples in the 56-75vol% compositional spread and Mo-(Si) S.S. These density values were then compared to the strengths for each composition on the same plot (Figure 18). This plot makes it clear that, while strength had little correlation with matrix volume fraction, it varied directly with theoretical density. On the other hand, this leaves the question of whether achievable density is dependent on

composition. In other words, should the 65%Mo samples necessarily have the highest density? Powder properties, although controlled via spray drying, may not be exactly the same for all compositions, so it would take a larger number of powder samples and specimens to answer this question conclusively. Such a determination is beyond the scope of this project.

It has been established empirically[25] that strength decreases exponentially with porosity, as given by:

$$\sigma_f = \sigma_o e^{-nP} , \tag{6}$$

or alternatively,

$$\ln \sigma_f = \ln \sigma_o - nP , \tag{7}$$

where σ_o is the theoretical maximum strength, σ_f is the fracture strength, n is an empirical constant (usually 4 to 7), and P is the percentage of porosity. A plot was made of the logarithm of strength versus porosity fraction (see Figure 19). According to the relation in equation (7), the trend should be linear with a slope equal to n and an intercept at the theoretical maximum strength. Although there is significant spread in the porosity data across all of the compositions, notice that individual compositions exhibit a tight fit to linear slopes. The y-intercept gives a theoretical maximum strength of 1320 MPa. The constant n accounts for the effects of pore size and distribution, which may be more influential than porosity percentage. For the same pore fraction, larger diameter pores will be more deleterious to strength than smaller, more disperse ones. This is due to the fact that larger pores increase stress concentrations, a mechanism that leads to a critical flaw size for a given load to failure. Microstructures in the interior of the bars (Figures

18, 19) reveal mostly spherical, isolated pores in the size range of 1-4 μm. This porosity is in the range that can be expected to be eliminated with subsequent HIPing.

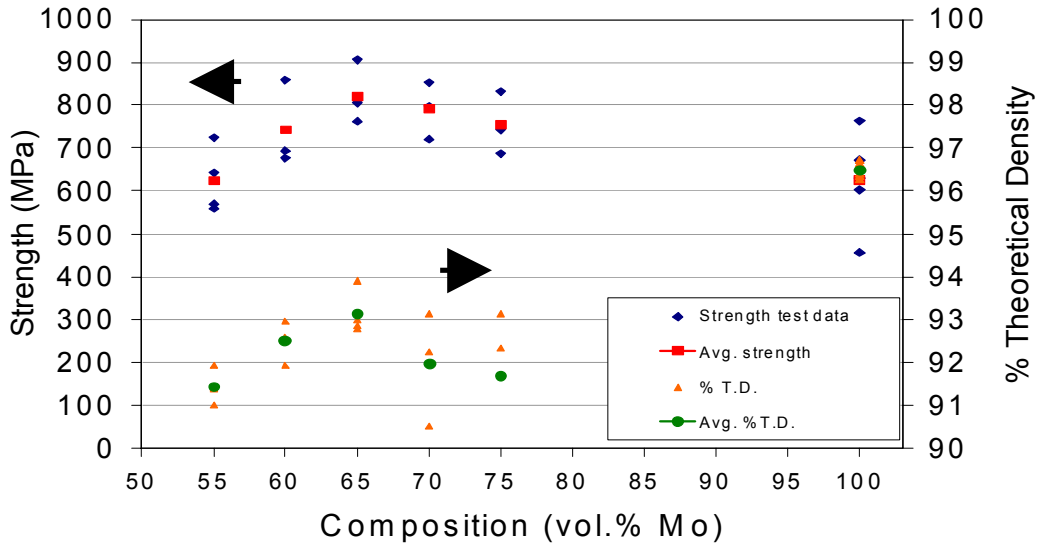

Fig. 18: Plot showing relationship between density and strength for several compositions

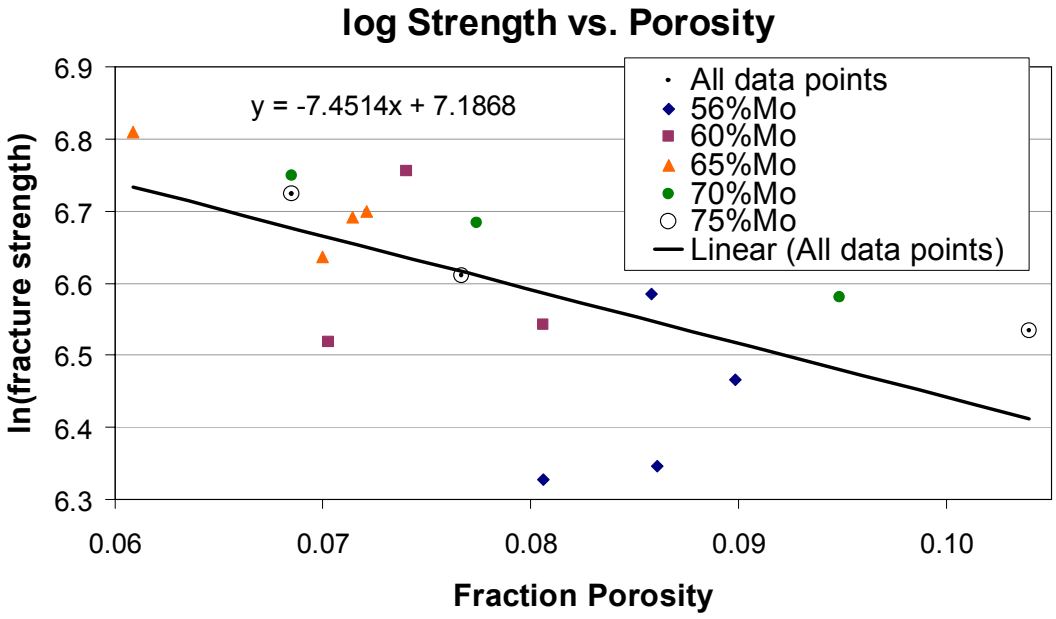

Fig. 19: Linear relationship between pore fraction and logarithmic strength

4.4 Processing Variables

4.4.1 Burnout Methods and Carbide Formation

The presence of molybdenum carbide has equivocal effects. As will be discussed in a later section, aluminum-containing samples show substantial formation of Mo_2C without a pre-fire burnout in air (Figures 33 and 34), and the strengths of these specimens are approximately half of those for bars that were burned out. Burnout for these specimens caused a marked and undeniable benefit to strength and ductility. However, other samples showed no difference at all or even detrimental oxidation effects due to an air burnout.

A systematic study of burnout methods was carried out, intended to answer definitively the question of which burnout method, if any, was optimal. In this experiment, samples of pure molybdenum (pureMo) and 65vol%Mo-3/1 (65Mo-3/1) were subjected to one of three treatments: no burnout, 300°C hold in a vacuum for two hours, and a 300°C hold in the Ar/H_2 furnace atmosphere for two hours. In both burnout cases, the average weight loss in the samples was around 1.85%, which corresponds to the binder content. XRD scans of these specimens (Figures 14 and 15) show negligible Mo_2C formation for any of the three treatments. However, notice in Figure 14 that the Ar/H_2 burnout (red curve) shows a reduction in the intensity of T2 peaks and an increase for A15 peaks (which is indicative of a change in the content of these phases). It is probable that the gases used in the furnace atmosphere contain oxygen impurities which would oxidize boron and silicon. The obvious explanation for a decrease in T2 formation would be the unavailability of boron, so one might assume that boron is preferentially oxidized, if

oxidation is indeed what occurred. The strength data also show no trend that correlates to the burnout method (Figures 16 and 17). In light of this study it was concluded that the best burnout method was none at all.

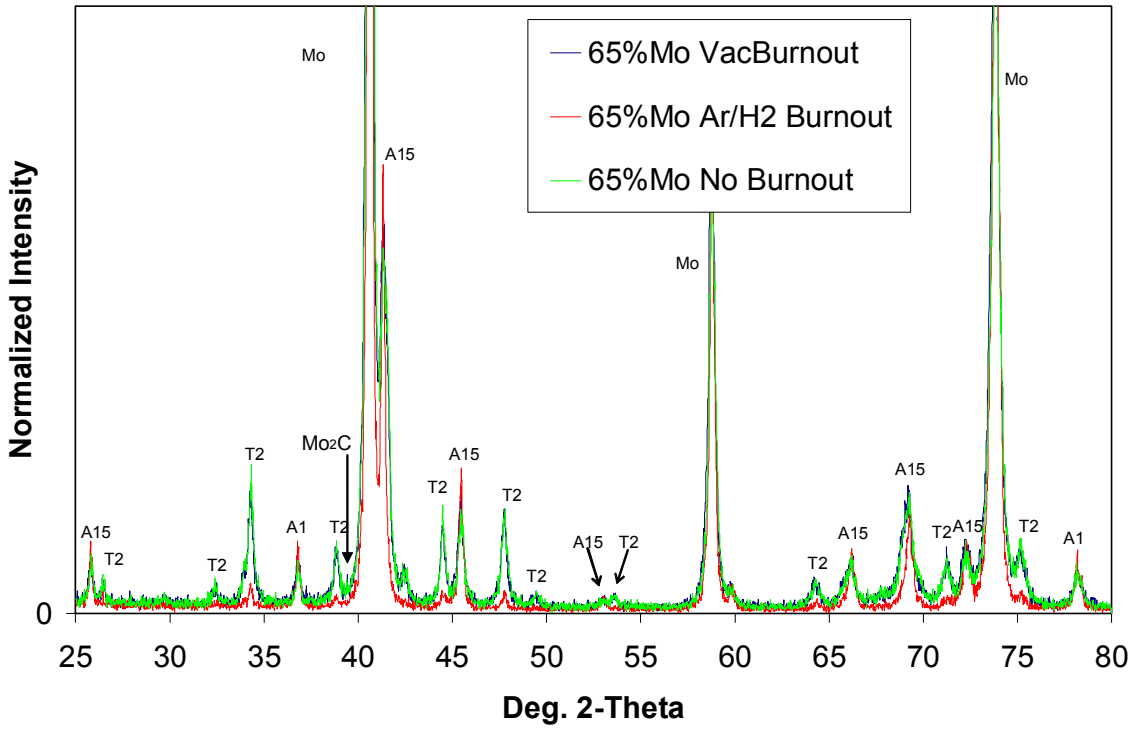

Fig. 20: XRD scan of 65Mo-3/1 specimens subjected to various burnout methods

4.4.2 Furnace Atmosphere

At the outset of the project, a 10%H_2, N_2 balance atmosphere was used for firing. [20] Although nitrogen is sufficiently inert, it was reasoned that using argon instead would facilitate decomposition of the nitrides based simply on Le Chatlier's principle, since nitrogen gas is a product of the decomposition.

Through thermogravimetric analysis (TGA) experiments, it was determined that in the N_2 atmosphere, molybdenum was forming a nitride at 900°C, which would then decompose back to Mo at 1100°C. This reaction causes an expansion of volume and was having a detrimental effect on fired densities. In light of this, the firing atmosphere was changed to 10%H_2, balance Ar.

Later on in the project, firing was producing consistently poor samples with high porosity and a rough surface finish, indicative of oxidation occurring in the furnace. Visual inspection of the furnace tube revealed a hairline crack which had been present for an unknown amount of time. The presence of a leak was evident in the inability to draw a full vacuum in the system. The tube was replaced and immediately a higher vacuum was attainable, indicating that the crack must have been the source of a leak of atmospheric oxygen into the furnace environment. For this reason, many specimens which had exhibited poor density and strength were suspect and were prepared and fired again.

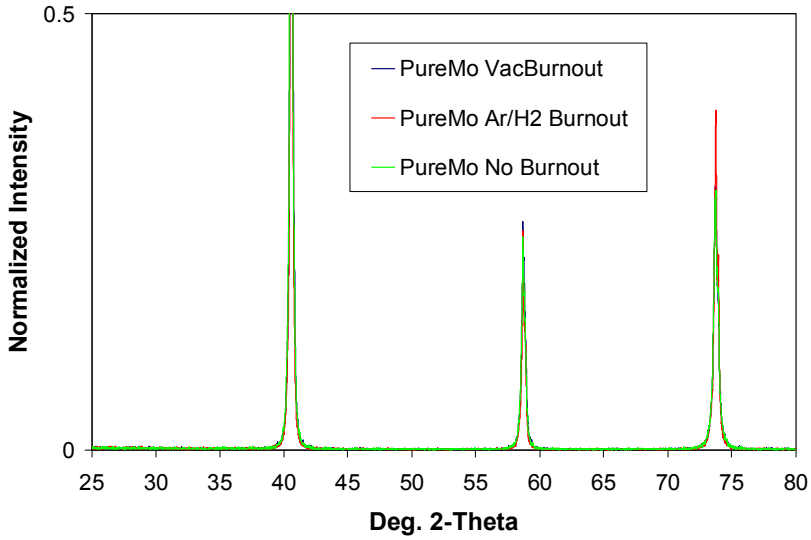

Fig. 21: XRD scan of pureMo specimens subjected to various burnout methods

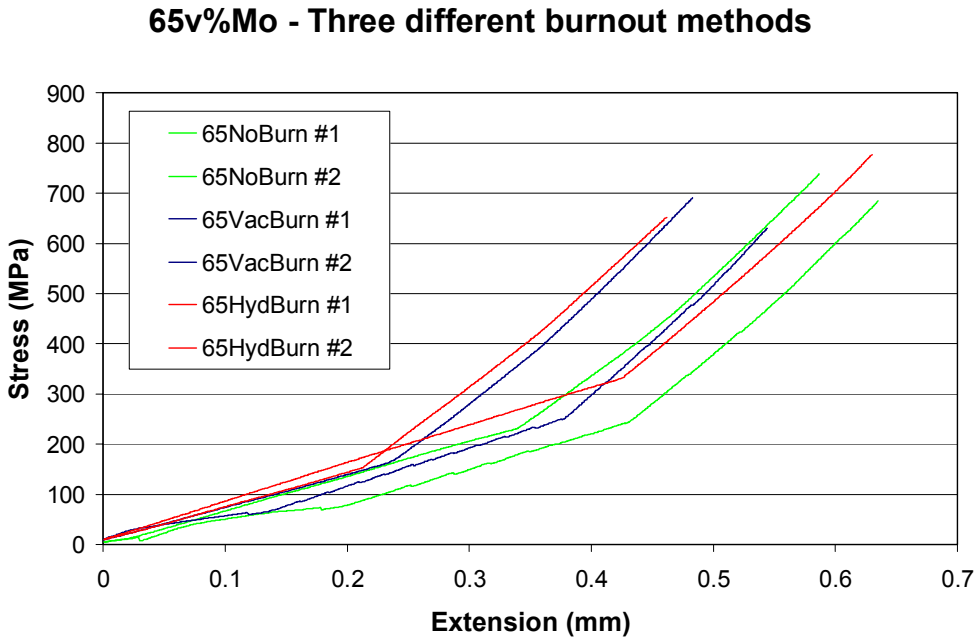

Fig. 22: Stress vs. displacement curves for 65Mo-3/1 compositions after various burnout methods

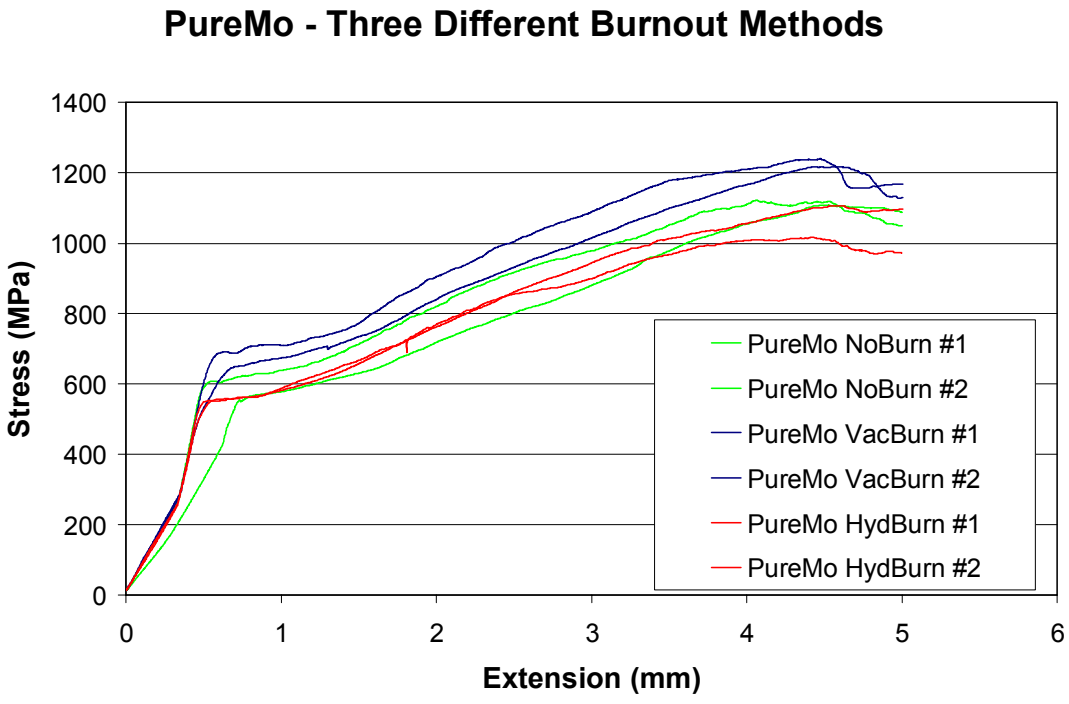

Fig. 23: Stress vs. displacement curves for PureMo samples after various burnout methods

4.5 Alloying Additions

4.5.1 Tantalum

It was thought that tantalum might improve ductility either because of its own inherent ductility or because of its highly reactive nature and tendency to getter oxygen and other elements. Two types of specimens were prepared: a Mo-6%Ta alloy (as a pure, "control" sample) and a Mo-Ta-Si alloy to observe its effect on the Mo_{ss} matrix.

The first batch of these alloys exhibited very poor density (the average was below 8.0 g/cm^3 for both compositions), with a rough surface finish and visible porosity. This was near the time when the cracked furnace tube was discovered, so the poor sintering of these specimens was attributed to oxygen impurities in the furnace. After replacing the tube and being reasonably sure that the atmosphere was as free of oxygen as possible, more tantalum-containing specimens were fired. These specimens turned out as poorly as the previous ones. Some micrographs and EDS element maps of these alloys are shown in Figures 24-26.

The brighter spots visible in Figure 24 are tantalum-rich regions. The microstructure seems to have little porosity, but the large region in the right half of the micrograph shows poor sintering. Such regions were visible across the whole surface. The first thing to notice in Figure 25 is that the bright Ta-rich spots also show concentrations of oxygen. This is evidence that Ta is oxidizing during firing, which may explain the poor sintering results. Notice also the mottled look in the electron image (Figure 25, top left). Some

dark regions surrounded by a lighter phase are apparent. This may suggest that tantalum or its oxides are segregating to grain boundaries, but the Ta and Mo maps do not reveal this clearly. XRD scans (Figures 27 and 28) of each sample show almost entirely pure Mo peaks. There are also minor peaks for some various oxides of Ta. Given the complex oxidation behavior of Ta, the peaks do not correspond to any particular stoichiometric oxide, but a mix of several.

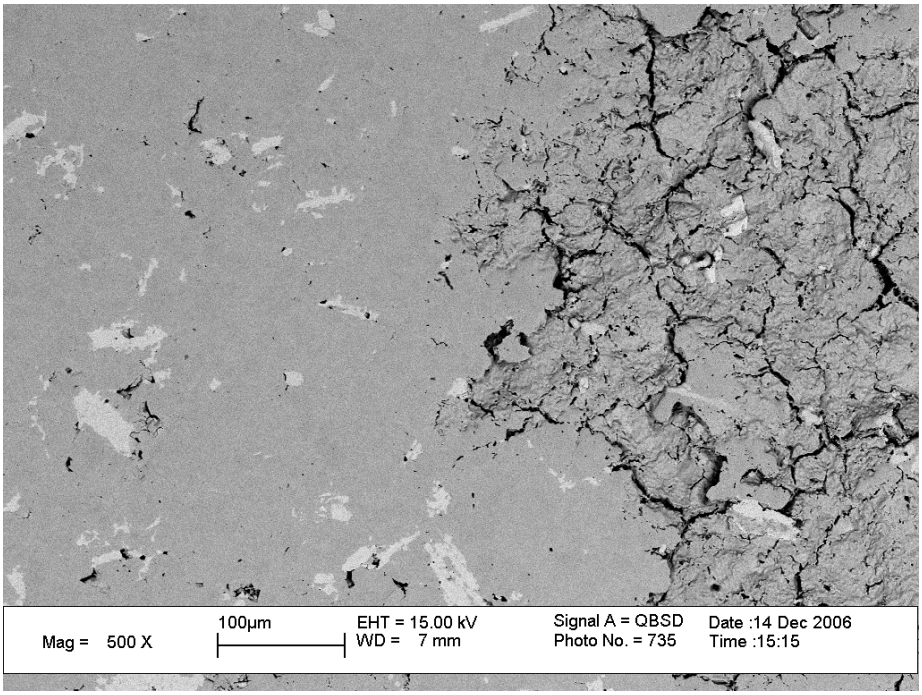

Fig. 24: Electron micrograph of Mo-6%Ta specimen. Tantalum is the light-colored phase

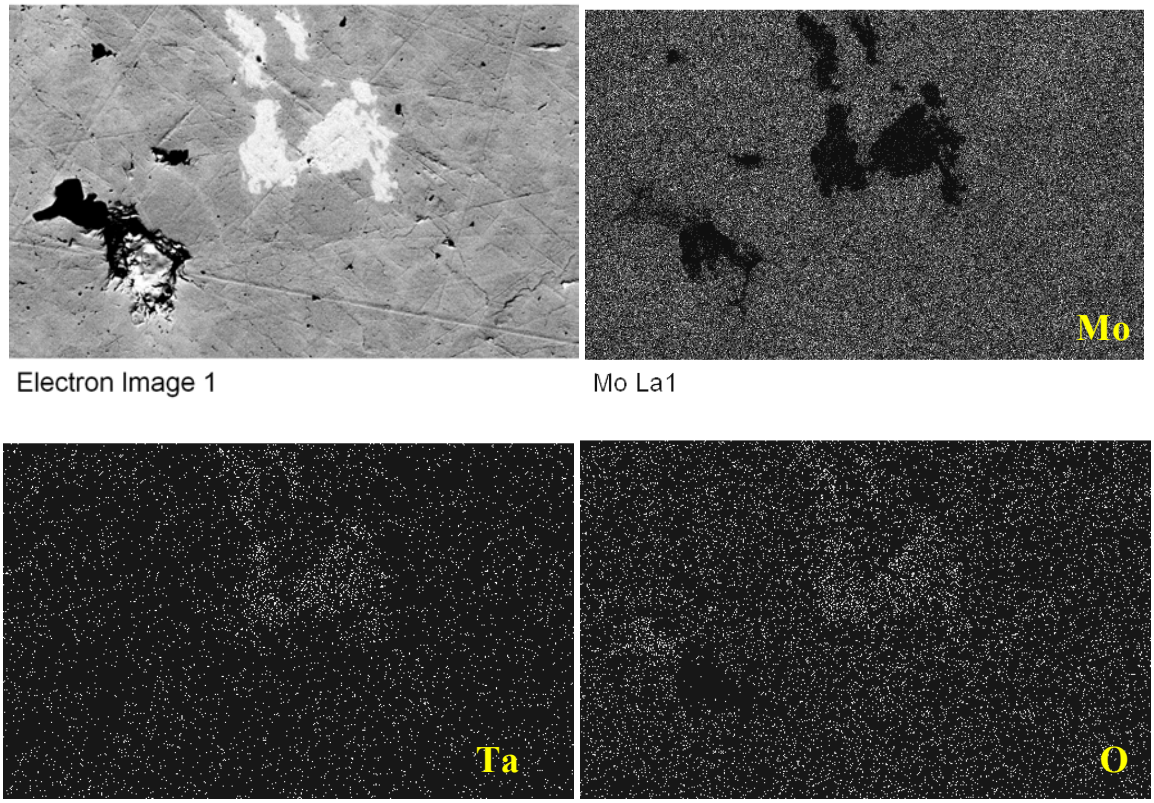

Fig. 25: EDS element maps for Mo-6%Ta alloy, clockwise from top left: backscattered electron image, Mo map, O map, Ta map

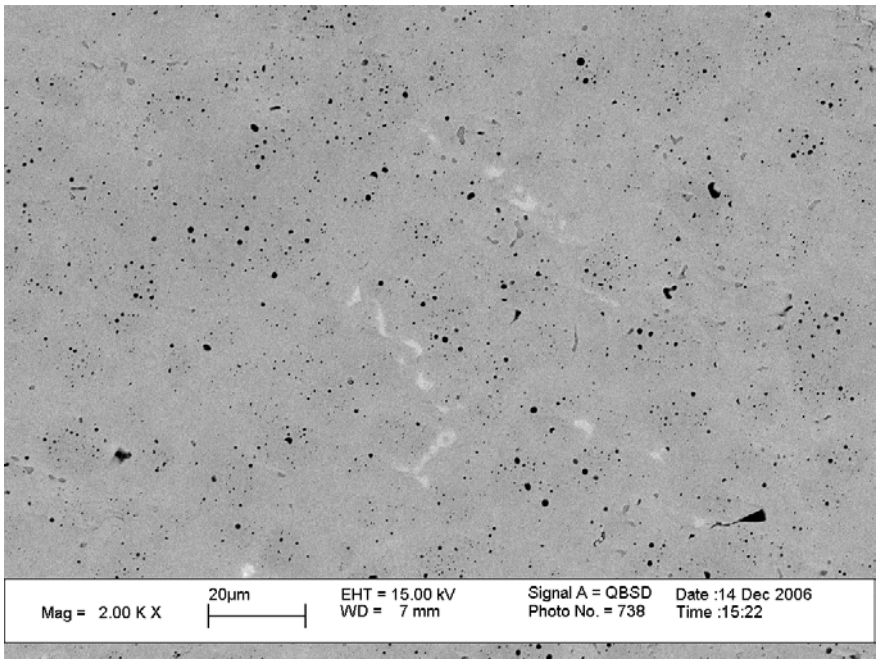

Fig. 26: Electron micrograph of Mo-Ta-Si alloy

The mechanical behavior of the Ta specimens was very poor. Ductility was expected, given the lack of solid solution hardening by silicon, but the porosity of the samples was much too high to exhibit this expected behavior. The apparent deviation from linear elasticity, i.e. the slump in the curves just prior to failure is best termed "graceful failure" and is a porosity effect rather than true ductility. This is the same case for the Mo-Ta-Si specimens (Figure 29).

A third attempt at firing Ta specimens was made. While other Mo-Si-B specimens in the same furnace run turned out fine, the Ta specimens still sintered poorly. In light of this, further studies of Ta addition were abandoned. There is apparently some kind of strong reaction occurring during firing that is damaging the specimens. Further investigation into Ta additions would necessitate in-situ monitoring during the furnace run or perhaps differential thermal analyses (DTA). Such a detailed analysis is beyond the scope of this project, particularly since it is now not expected that Ta will bring about a significant improvement in mechanical or oxidative properties.

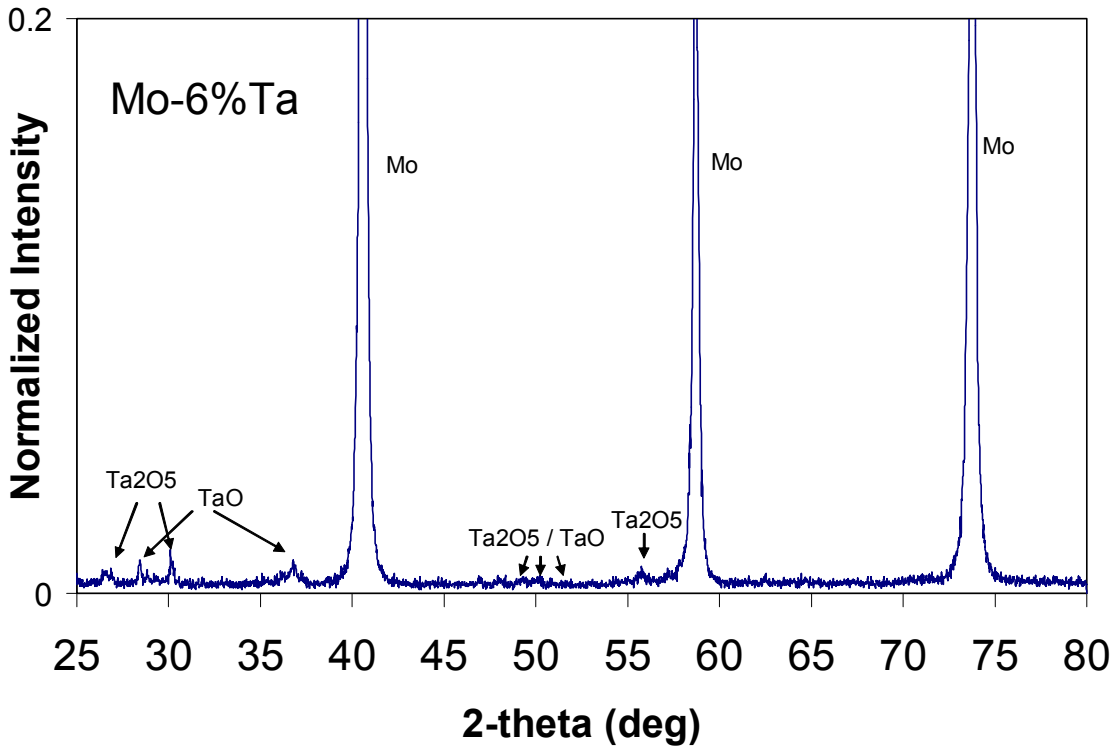

Fig. 27: XRD scan of Mo-6%Ta sample, intensity normalized to highest Mo peak

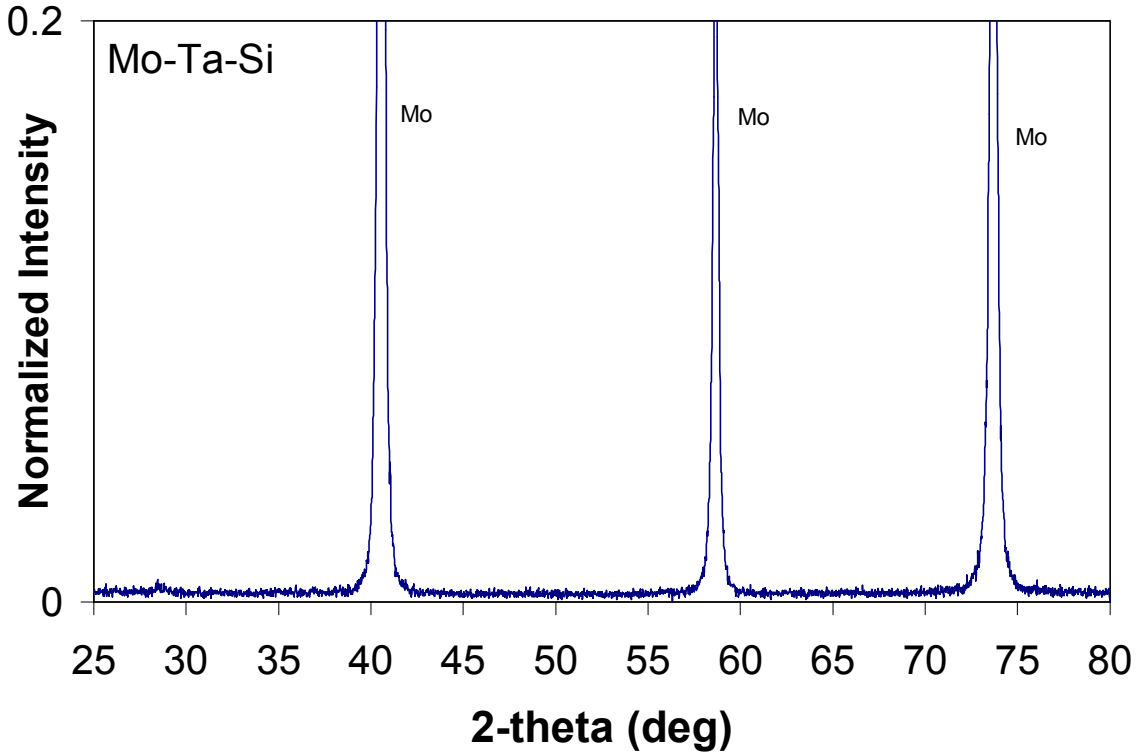

Fig. 28: XRD scan of Mo-Ta-Si sample, intensity normalized to highest Mo peak

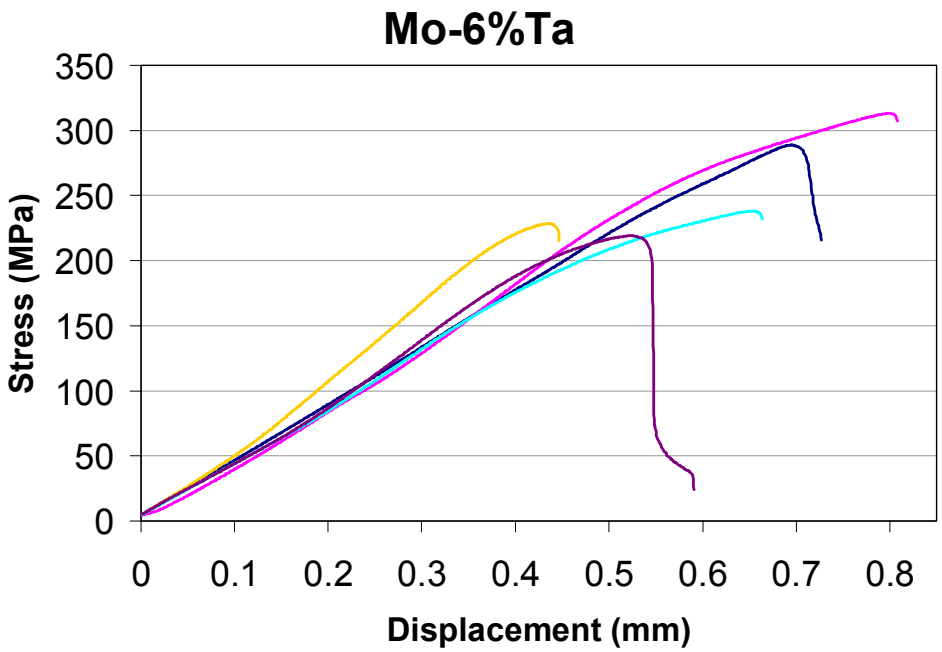

Fig. 29: Stress vs. displacement curves for Mo-6%Ta specimens

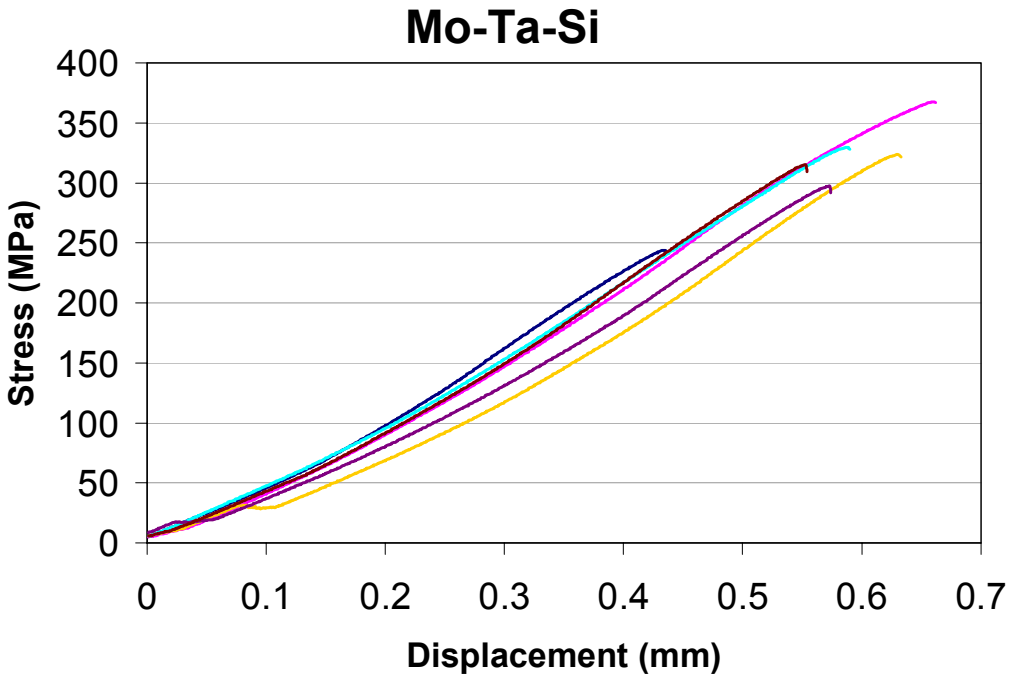

Fig. 30: Stress vs. displacement curves for Mo-Ta-Si specimens

4.5.2 Aluminum

Aluminum was chosen as an additive to Mo-Si-B alloys with the intention of improving oxidation resistance via the formation of mullite ($Al_6Si_2O_{13}$). Initial background research (see Mo-Al-Si phase diagram in Figure 31) showed that aluminum is isostructural with silicon in the A15 phase and will substitute at any fraction. For melt processing techniques, adding aluminum is all but impossible because of its evaporation at the extremely high temperatures involved. But powder processing circumvents this problem – the vapor pressure of aluminum is only around 200 Pa (.002 atm) at 1600°C, the sintering temperature used for the nitride-based synthesis process. An initial trial composition (the green dot in Figure 32) revealed that Al shifts the solubility along the (Al, Si) axis and changes the boundaries of the MoB_2, T2, Mo_{ss} compatibility triangle. As indicated in Figure 32, the trial composition was selected in an analogous position to a 56Mo-3/1 composition. But XRD analysis of this composition revealed the phases present were Mo_{ss}, T2, and MoB_2. Accordingly, the compatibility triangle for these phases is shifted in the projected Mo-(Al, Si)-B quasi-ternary (see Figure 32). The most promising aspect is that the diagram suggests Al should to reduce the solubility of Si in Mo, which is essential for lowering the DBTT the alloys. Two compositions were compounded using Mo, Al, Si_3N_4, and BN powders and prepared by the milling and spray drying technique described in the experimental procedure section and fired at 1600°C for six hours. The first composition, dubbed Mo-(Al,Si,B) S.S., contains sufficient alloying elements to saturate the matrix. The second, 70Mo-(Al,Si,B), was intended to contain 70vol% of the Mo_{ss} matrix. Each composition substituted Al for Si in a 3:1 ratio. The phase content of these compositions is summarized in table 3.

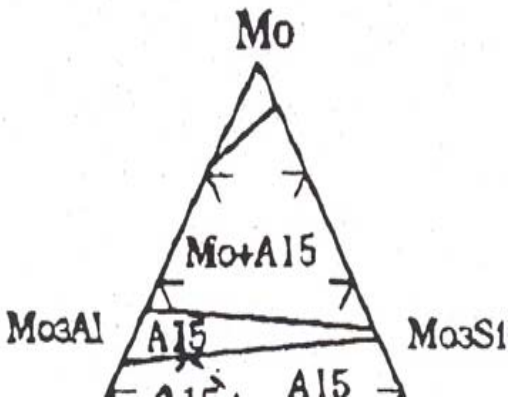

Fig. 31: The Mo-rich corner of the Mo-Al-Si phase diagram showing complete solubility of aluminum in A15, [26]

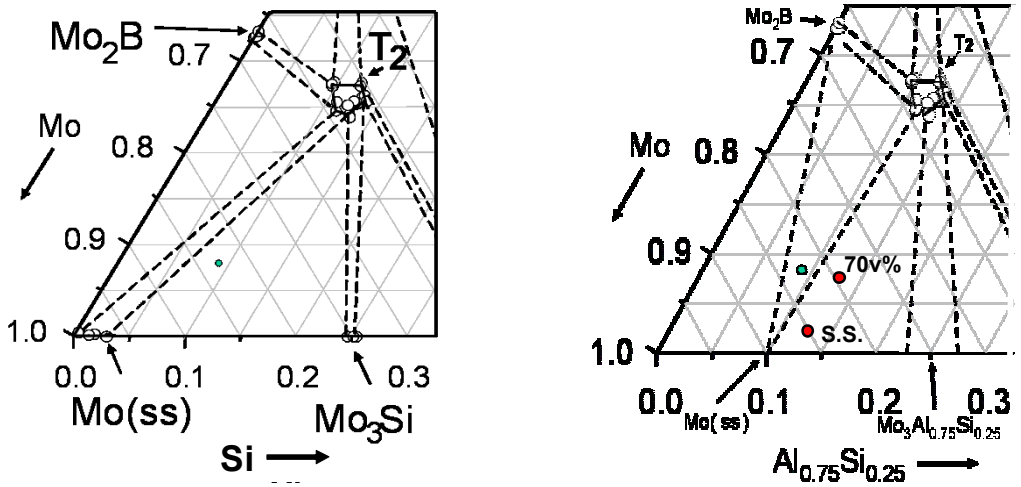

Fig. 32: Mo-Si-B ternary phase diagram (left) compared with projected Mo-(Al, Si)-B quasi-ternary diagram (right); location of compositions as indicated, after [4]

The XRD scans for the aluminum specimens are shown in Figures 33 and 34. The strong peaks for aluminum overlap with those of the intermetallic phases, so it is difficult to determine if any aluminum metal is present. What is known is that most of the aluminum is present as aluminum oxide, either formed during firing or originating in the raw powders (aluminum oxide cannot be reduced by hydrogen). Assuming that most of the aluminum not oxidized goes into solid solution within A15, it would be undetectable as a

distinct phase anyway. Perhaps some experiments with pure Mo and pure A15 could reveal the solubility behavior of aluminum, but these are beyond the scope of this project.

The microstructures of the Al-containing samples are similar to the previous 3/1 compositions, at least with respect to the intermetallic phase structure. As shown in Table 3., the 70v% composition was projected to contain about 35vol% intermetallics while the S.S. was projected to contain about 15vol% intermetallics. Intermetallic content appears somewhat higher than expected for the solid solution specimens (Figures 35 and 37), but the 70v% Mo specimens (Figures 36 and 38) show a corresponding slightly higher intermetallic area fraction. EDS element maps (Figures 39 and 40) reveal that black regions which appear as voids are actually pockets of aluminum and/or aluminum oxide. This is strong evidence that the aluminum is not dispersing homogeneously, but rather segregating as discrete particles. In this case, it cannot be assumed that the system is at equilibrium or that any substantial amount of aluminum has been dissolved in the matrix. One possibility is that the oxide layer around the aluminum particles is containing the Al, preventing it from dispersing, but this is unlikely in light of the success of industrial processes such as the unidirectional oxidation of aluminum. In this process the oxide layer develops cracks through which fresh aluminum can migrate freely. The particle size of the aluminum was 1-5 microns, which is two to ten times larger the other raw powders. It is likely that the dispersion seen in the micrographs (Figures 35 through 38), with a size range of 1-10 microns, is as homogeneous as achievable with this aluminum powder, suggesting, then, that nano-sized Al powder should be used. However, such high surface area aluminum would be prone to extensive oxidation. This aluminum oxide could not be

reduced and would not allow dissolution in or reaction with Mo to produce the desired phases.

The first batches of Al-containing specimens were subjected to different pre-fire treatments: half were burned out, half not. In this case, the burned-out samples showed a marked difference in density: an average 90% T.D. versus 80% for those not burned out. Significant carbide formation is seen in the XRD scans of samples without burnout (Figures 33 and 34). This is contradictory to the aforementioned burnout study done on pure Mo and 3/1 samples, which showed almost no difference in carbide content or density or strength. Why carbide formation is so enhanced and density so reduced for Al-containing specimens in absence of a pre-fire burnout is puzzling. Further confounding this issue is that samples produced from a second, presumably identical batch of powders did not show such substantial carbide formation with or without burnout. It is possible that the purity of the furnace atmosphere plays a role. The only certainty is that burnout is beneficial for the density and resultant strength of Al-containing specimens.

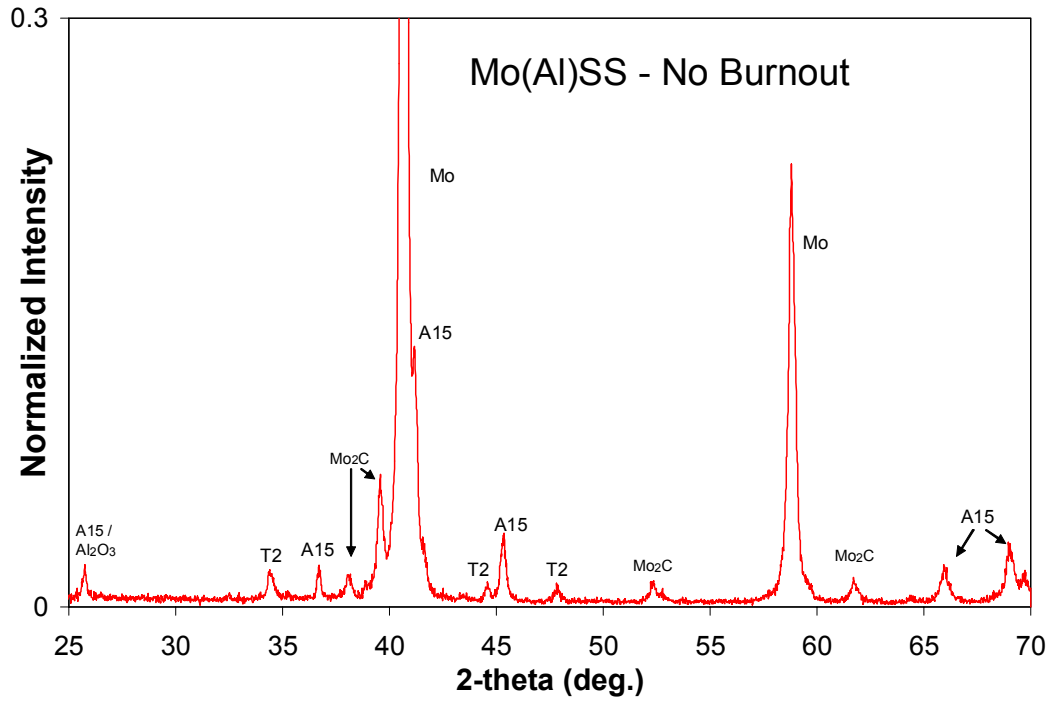

Fig. 33: XRD scan for Mo-(Al,Si,B) S.S. sample; note significant Mo_2C formation without burnout

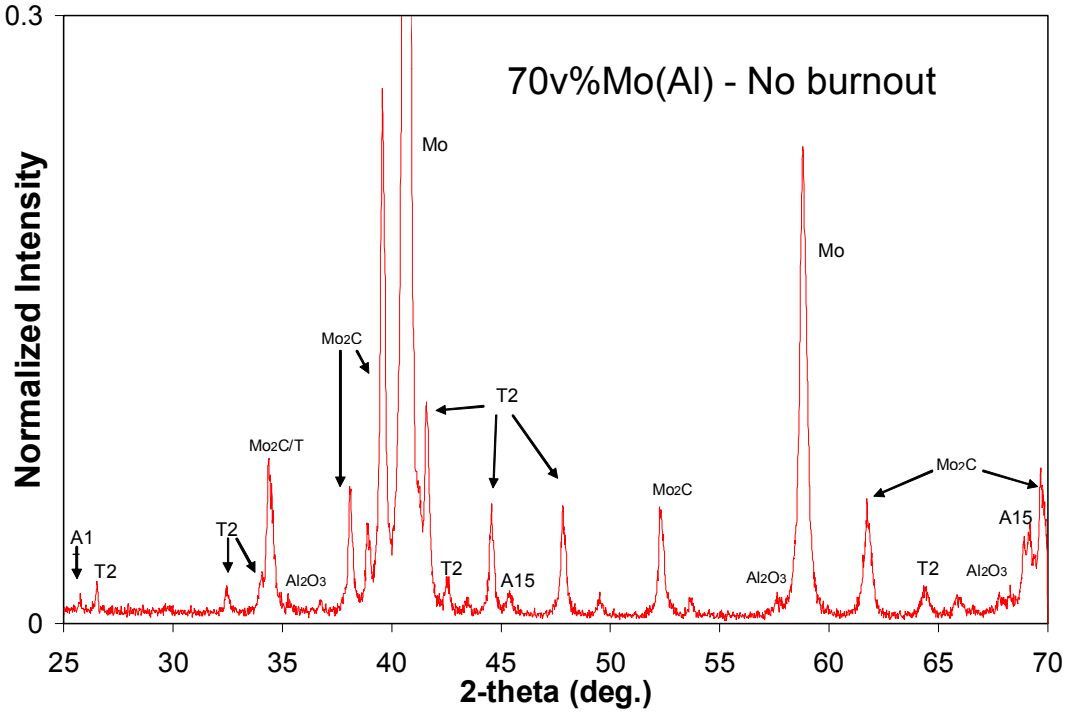

Fig. 34: XRD scan for 70Mo-(Al,Si,B) sample; note significant Mo_2C formation without burnout

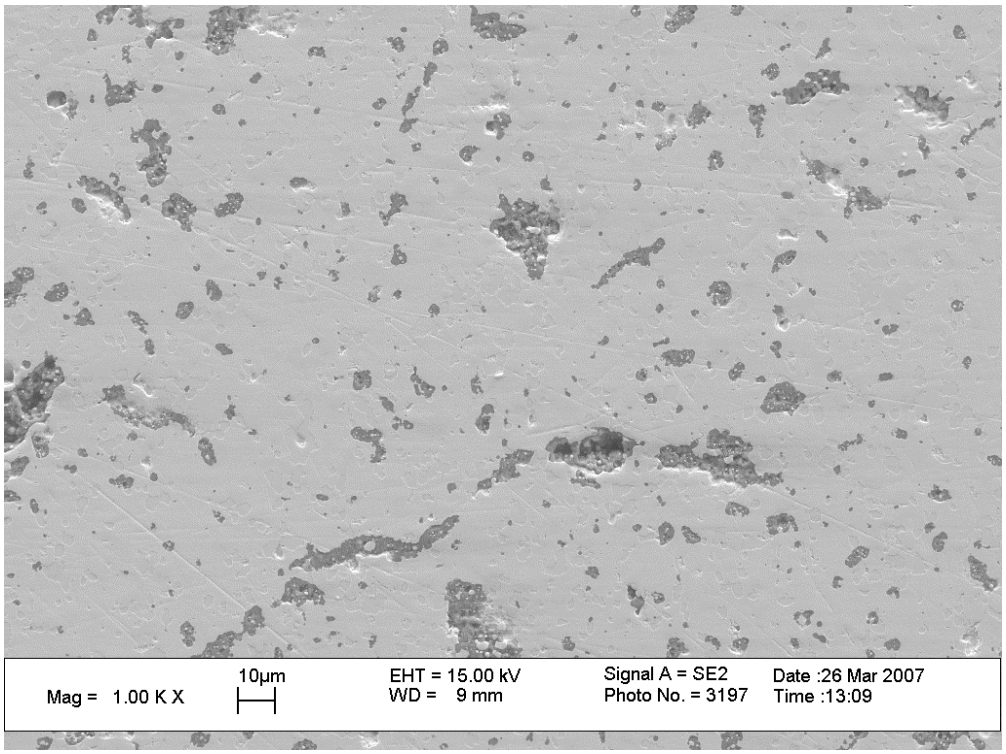

Fig. 35: Secondary electron micrograph of Mo-(Al,Si,B) S.S. at 1000x; darker regions are clusters of Al and Al_2O_3

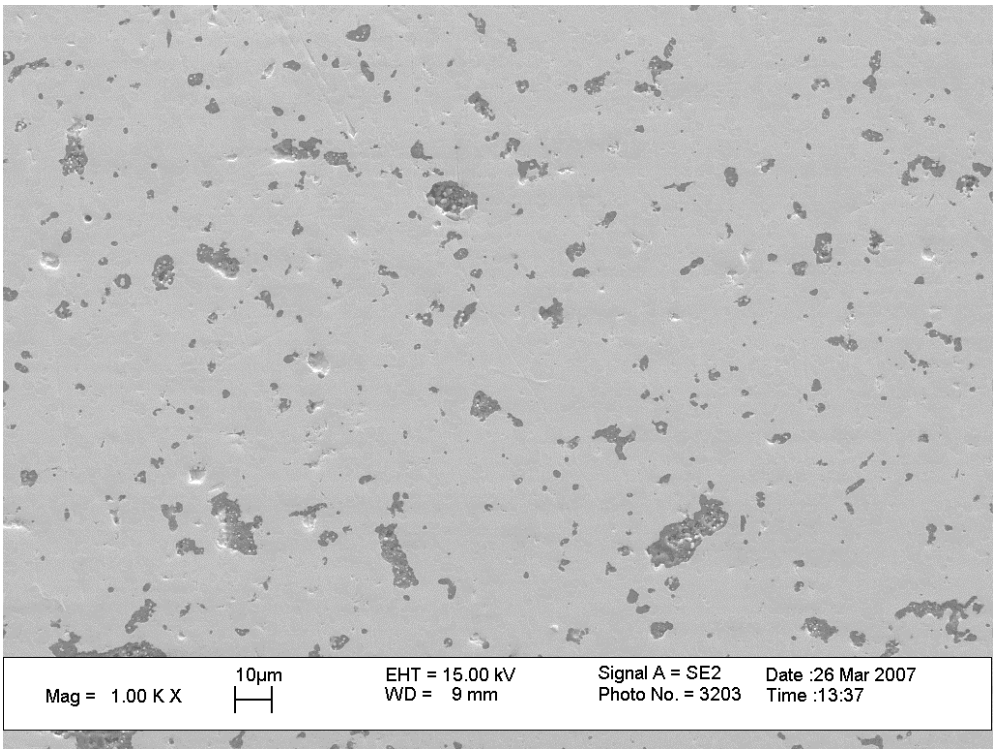

Fig. 36: Secondary electron micrograph of 70Mo-(Al,Si,B) at 1000x; darker regions are clusters of Al and Al_2O_3

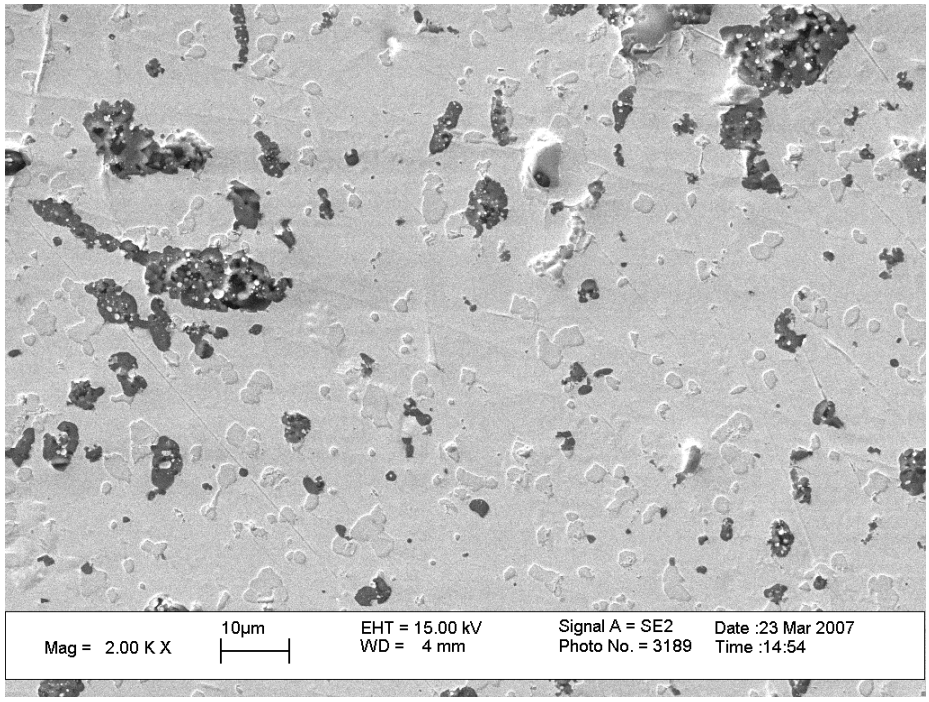

Fig. 37: Secondary electron micrograph of Mo-(Al,Si,B) S.S. at 2000x. Phase contrast seems to be a result of surface relief – the depressed regions are the intermetallics. Darkest regions are clusters of aluminum oxide.

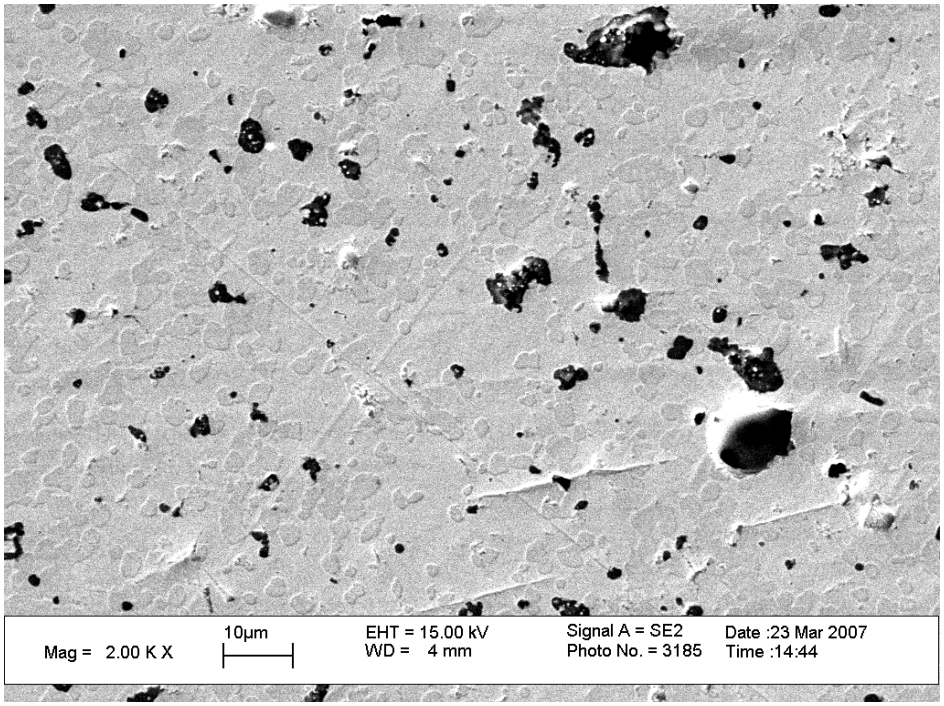

Fig. 38: Secondary electron micrograph of 70Mo-(Al,Si,B) at 2000x. Phase contrast seems to be a result of surface relief– the depressed regions are the intermetallics. Darkest regions are clusters of aluminum oxide.

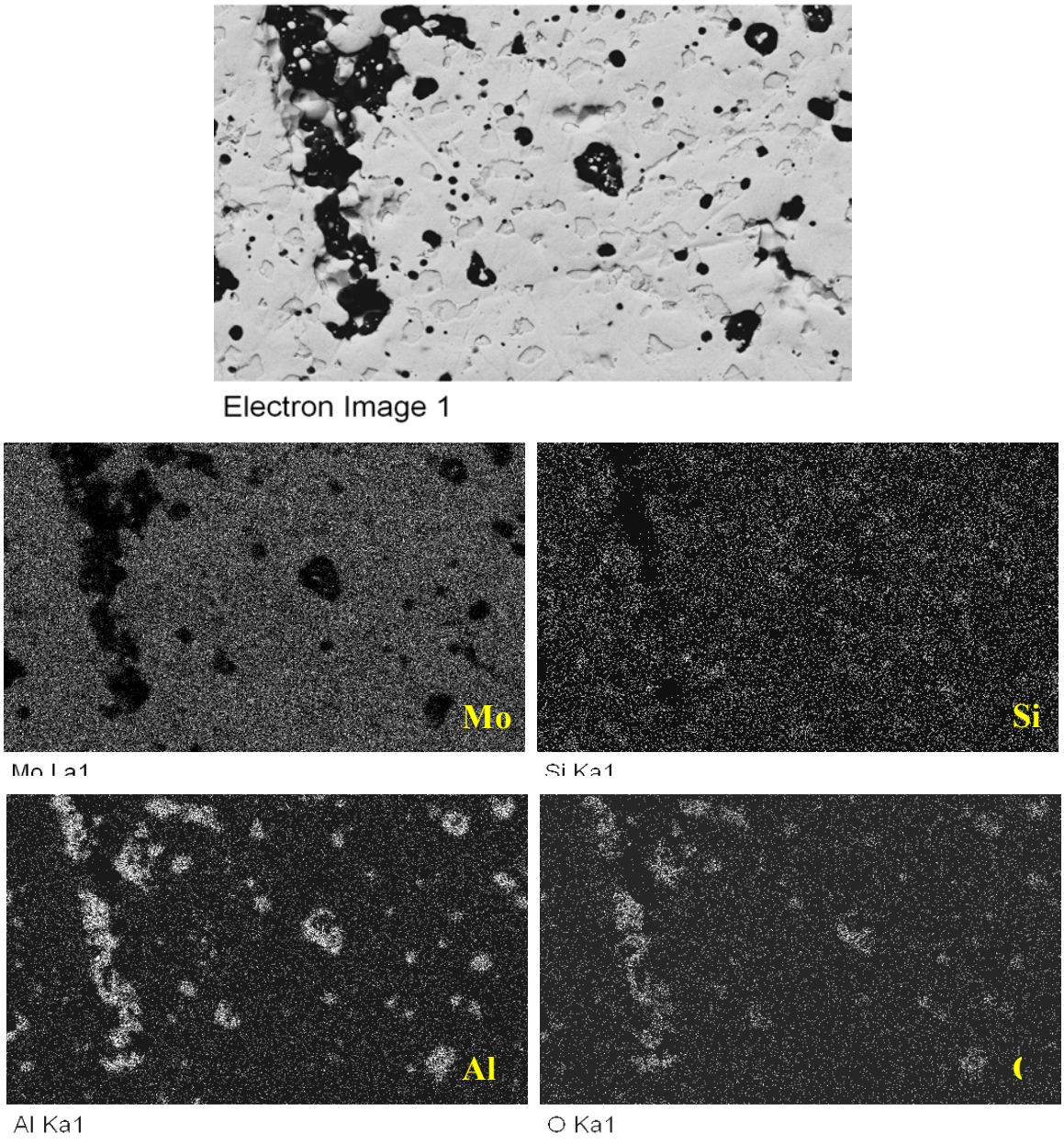

Fig. 39: EDS map for Mo-(Al,Si,B) S.S. specimen, elements as noted

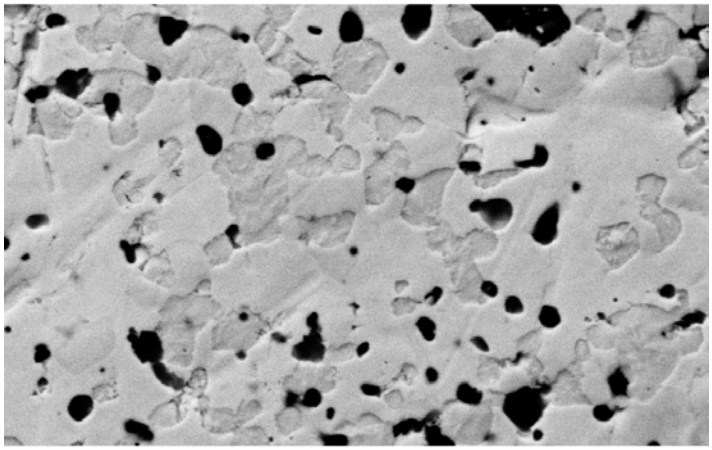

Electron Image 1

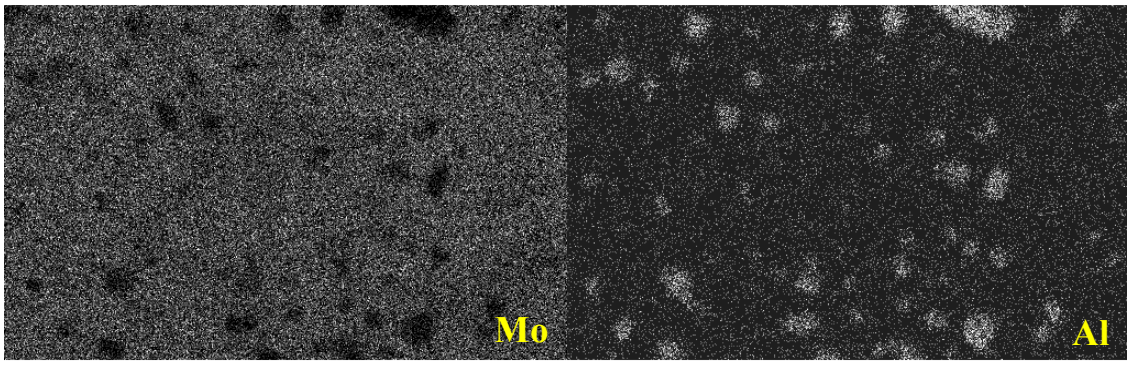

Mo La1 Al Ka1

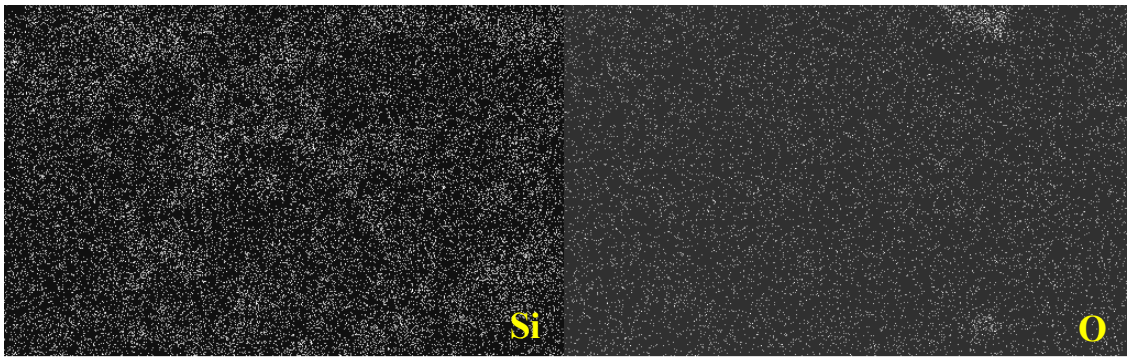

Si Ka1 O Ka1

Fig. 40: EDS map for 70Mo-(Al,Si,B) specimen, elements as noted

Recal that the first Al-containing powders prepared (referred to as “old powder”) had not been energetically milled in the paint shaker, which may have left intact coarse agglomerates that would not disperse. A second batch of Al-containing powders was prepared using the same procedure, except this time with a 60-minute paint shaker cycle just prior to spray drying (hereafter referred to as “new powder”). Also, in an attempt to induce equilibrium, the firing temperature was raised 50 degrees to 1650°C for samples prepared with the new powder.

These new samples achieved slightly better densities than the first batch. The average for burned-out specimens was 90.6% T.D. and for those not burned out, 82.5% T.D. Qualitatively, these had a smoother, shinier surface finish with less visible porosity. The microstructures of samples prepared from the new powder were identical to those from the old powders. Despite these new samples being made of the same powder compositions and fired under the same conditions as the old ones (other than a 50° temperature difference), XRD phase analysis reveals very little molybdenum carbide having formed, regardless of burnout treatment. On the other hand, there is an undeniable improvement in density with burnout, as has been the case with every batch of Al-containing specimens prepared. To understand carbide formation and what is happening during binder burnout and firing might require some coupled TGA and DTA experiments to observe the temperatures at which binder decomposition and other reactions take place. For now it must be concluded that binder burnout is necessary for the Al-containing samples.

Figure 41 shows the 200°C stress versus displacement curves for the first batch of Al-containing specimens prepared from the old powder. Here the benefit of burnout is most evident. The strength values for Mo(Al)SS specimens (green curves in Figure 41) are the highest observed for any Mo-Si-B composition tested. The curves even show the slightest deviation from linearity just before failure. This inspires confidence that elevating the test temperature by just 100-200°C would bring about substantial ductility in the Al-containing specimens. Additionally, even a brittle material may be useful if it possesses such a high strength. That the solid solution specimens exhibit such a superior strength to the 70vol% ones is probably a result of the difference in their average densities. The abrupt change in slope of the curve around 160 MPa is a compliance effect in the four-point bending jig and does not reflect any anomalous behavior of the specimens.

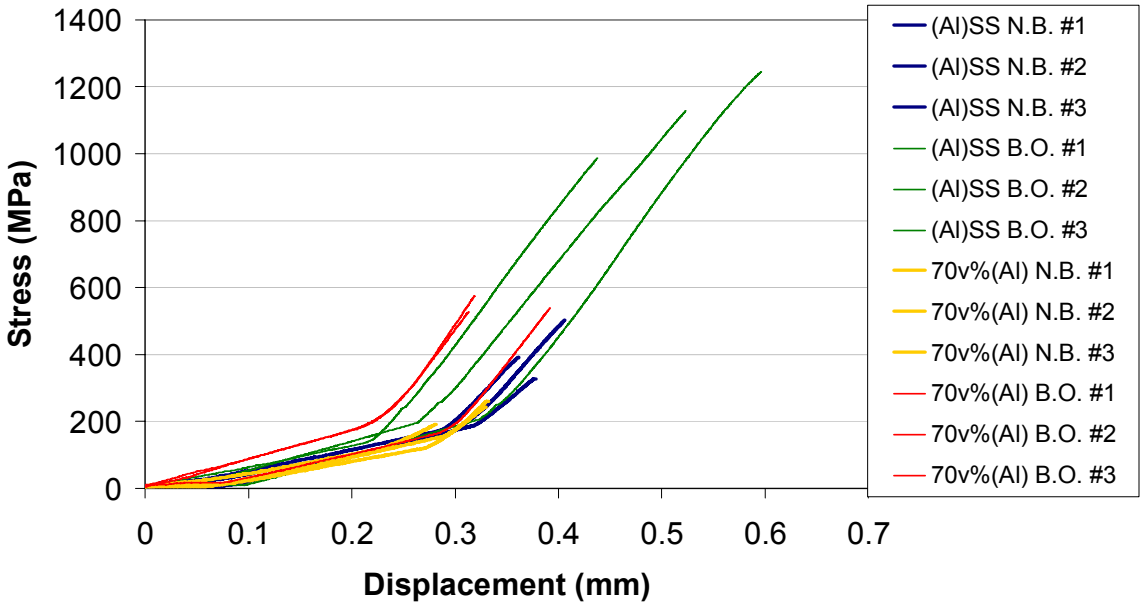

Fig. 41: Stress vs. displacement curves (corrected for compliance) for Al-containing specimens at 200°C which highlight the benefits of a pre-fire burnout in air.

The XRD scans for the Al samples made from the new powder are shown in Figures 42 and 43. These do not show substantial deviation from the original batch. Molybdenum carbide formation is more evident in the 70Mo(Al) new powder samples but in both compositions is less prevalent than in the old powder batch. However, notice that burnout brings about a significant reduction in the A15 peaks. A plausible explanation for this is that the oxidation of silicon during the burnout cycle leaves less free silicon available for intermetallic reactions. This effect was also suspect when a batch of Mo-0.67%Si S.S. samples turned out surprisingly ductile. It was reasoned that the silicon which would normally embrittle the Mo had oxidized out of solid solution and formed isolated glassy silica inclusions.

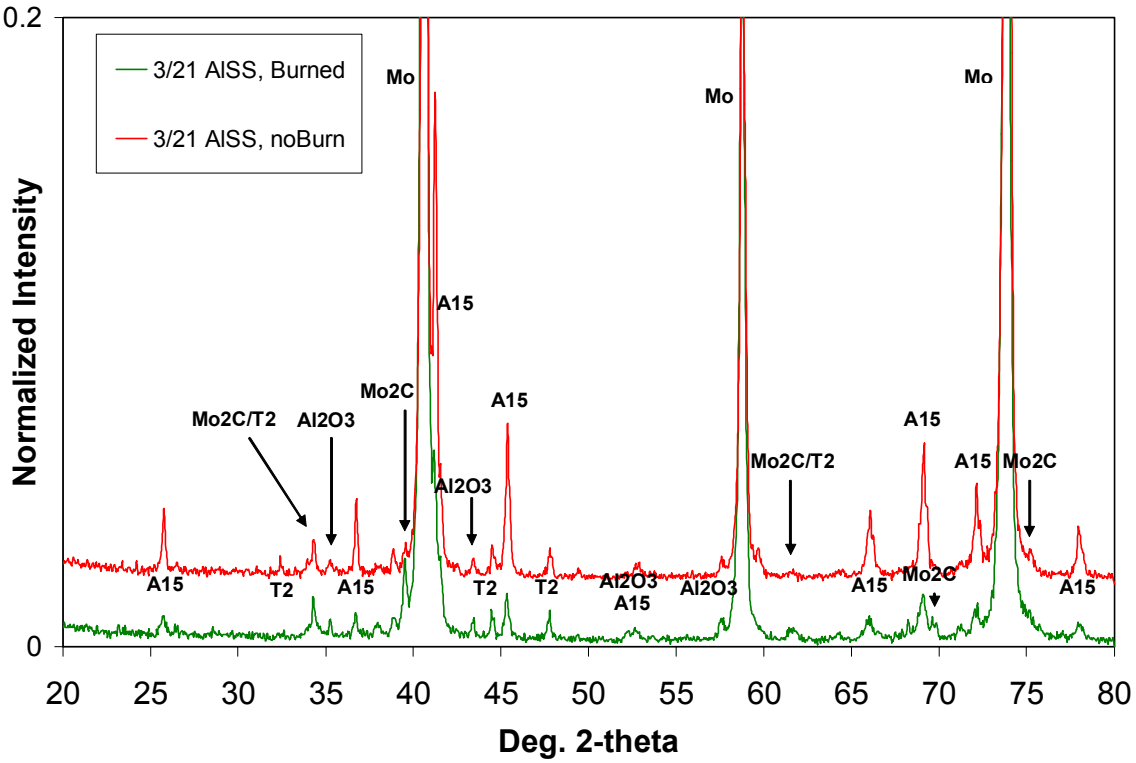

Fig. 42: XRD scan for new powder Mo-(Al,Si,B) S.S. specimens with and without burnout

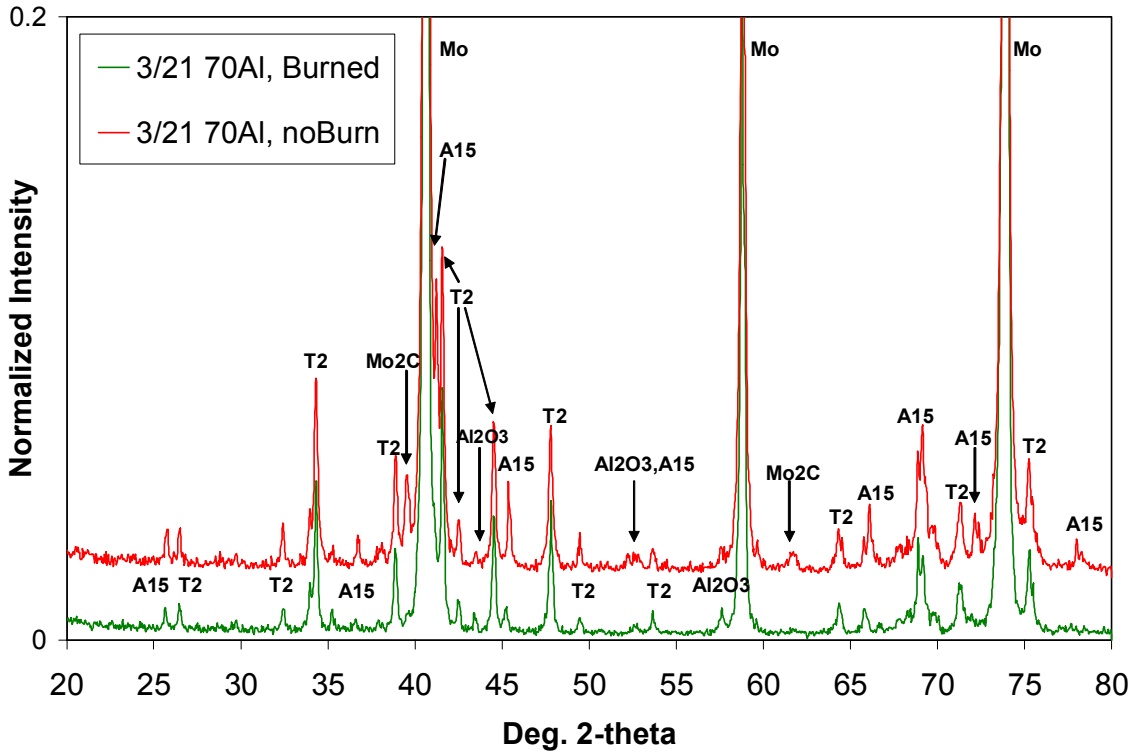

Fig. 43: XRD scan for new powder 70Mo-(Al,Si,B) samples with and without burnout

Bend testing of the new powder samples revealed more similar and consistent behavior between compositions and burnout treatments (see Figures 44 and 45). Referring back to the XRD scans in Figures 42 and 43, notice that carbide formation is more prevalent in the 70Mo(Al) specimens than for the solid solution specimens. And then notice in Figure 45 the significant difference in strength between burnout treatments for the 70Mo(Al) specimens. It is tempting to attribute this to a density difference between burnout treatments, which is indeed significant. However, as seen in table 5, the difference in densities between burnout treatments for both compositions is similar. If an 82% theoretically dense 70Mo(Al) specimen has an average strength about 250 MPa lower than a 90% theoretically dense one, then why is a correspondingly large discrepancy not

seen with the Mo(Al) S.S. specimens? This would lead to the belief that the presence of molybdenum carbide is certainly a detriment to strength.

Table 5: Comparison of average theoretical densities for Al-containing specimens

Average %T.D.		
	Mo(Al) S.S.	**70Mo(Al)**
Burned Out	90.59	90.84
No Burnout	83.41	81.97

These observations on aluminum addition to Mo-Si-B leave many questions unanswered, but the results are interesting nonetheless. Such additions are undoubtedly beneficial to low temperature strength and similar behavior is expected at high temperatures. Additionally, it is believed that aluminum could only help oxidation behavior. The next important steps in the investigation are to enhance dispersion of aluminum in the alloys and to understand the effects and mechanisms of burnout and carbide formation.

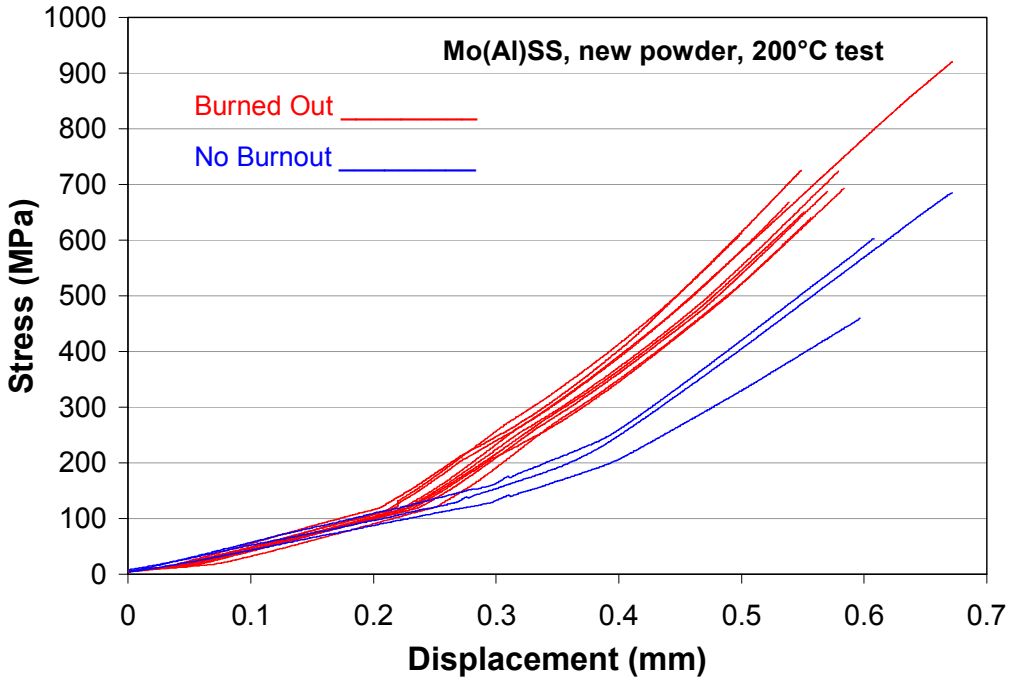

Fig. 44: Stress vs. displacement curves for Mo-(Al,Si,B) S.S. specimens from new powder

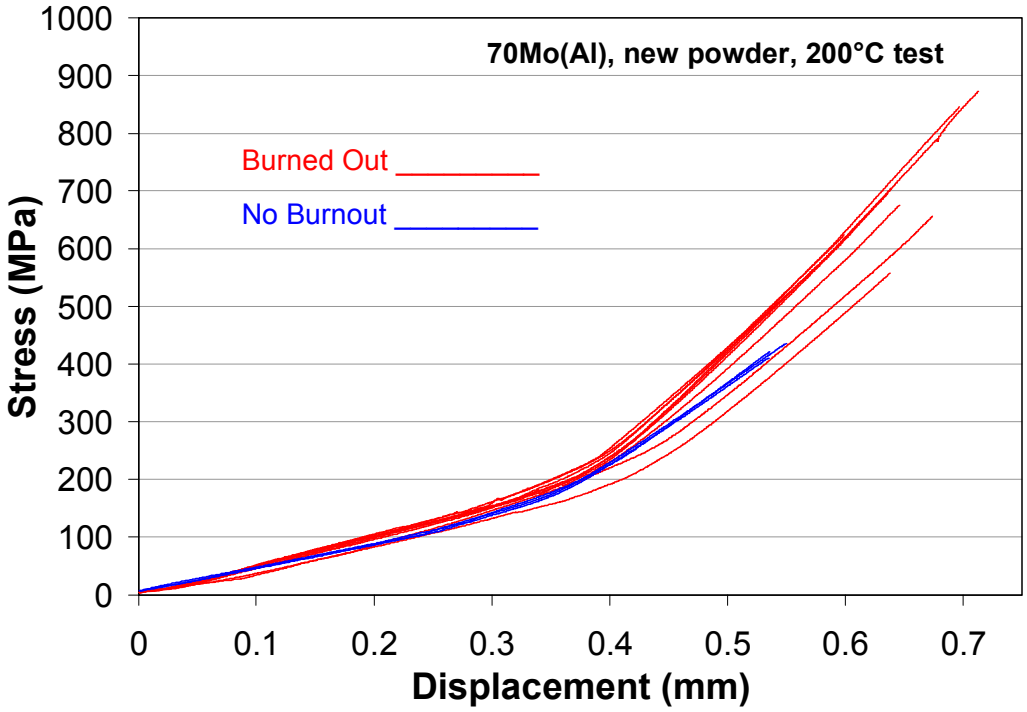

Fig. 45: Stress vs. displacement curves for 70Mo-(Al,Si,B) specimens from new powder

CHAPTER 5

CONCLUSIONS AND RECOMMENDATIONS

The nitride-based reactive sintering route has shown promise as a viable method of producing Mo-Si-B alloys. Among the numerous advantages of this processing route is scalability and use of common industrial methods as well as ease of compositional adjustments and alloying additions.

Although the quest for ductility in Mo-Si-B alloys continues, the specimens produced in this project exhibited exceptionally high strengths, exceeding those reported in previous literature. In any case, a method for producing fine-grained, high-strength and highly ductile molybdenum metal has been presented. These methods could probably be applied to other refractory alloy systems. In spite of the poor ductility observed in the Mo-Si-B samples, those in the turbine blade industry acknowledge that a brittle but very strong material is much better than a weak one.

Although not the focus of this investigation, oxidation properties of these alloys are at least as important as their mechanical behavior. Oxidation experiments have been proceeding in parallel with this work. Ultimately, these separate efforts will need to converge in order to reach the optimal compromise between mechanical properties and oxidation stability.

The onset of any ductility in Mo-Si-B alloys has commonly been found around 400°C, so the available thermal testing equipment in this project could not attain temperatures high enough to observe any change in DBTT. The next logical step in mechanical characterization, given the unlikelihood of imparting room temperature ductility in the Mo-Si-B system, is to begin high-temperature testing of the alloys. A preliminary step toward this end might be to find a way to press or machine dog-bone tensile specimens. Also, perhaps three-point bending would be a better method for simple ductility determination, as this is what was used in most of the literature surveyed.

As mentioned in the literature review, the literature is lacking a systematic study of solubility of silicon and boron in molybdenum and their effects on ductility and strength. The nitride-based processing method could be useful for undertaking such a study, since what is added to the slurry mixtures in the beginning shows up entirely in the fired sample. As an example, five levels of silicon and five levels of boron addition could be mechanically tested at room temperatures to high temperatures to determine their effect on DBTT. On the other hand, Mo-Si-B alloys are going to contain some minimal amount of silicon – likely around 3 wt% – so the effects of Si at levels lower than this are irrelevant. Perhaps an atomistic study of silicon dissolution and its effect on the lattice and dislocation interaction could lead to methods to reduce its solid solution hardening effect.

Aluminum additions show interesting, if not promising, results. These certainly warrant more investigation, particularly into improving dispersion of aluminum and studying

phase formation. Thermal analysis of the reactions would be first on the list if work were to continue with aluminum. A search of available aluminum compounds did not reveal an aluminum precursor such as AlN that would protect aluminum from oxidation but decompose during firing. Trial experiments with AlN showed that it is stable even up to 1700°C. However, this does not rule out the possibility that some suitable aluminum precursor compound might exist.

In any case, the application of Mo-Si-B alloys will entail a large change in engine design and operating characteristics. Engineers might have to switch from a fail-safe to a damage-tolerant design paradigm. Already Pratt & Whitney is considering these alloys for use in static parts such as heat shields, so there is hope for their commercial potential.

REFERENCES

[1] J.H. Schneibel. "Beyond Nickel-Base Superalloys". Proc. Thirteenth International Conf. on Processing and Fabrication of Advanced Materials (PFAM XIII), Singapore, Dec. 6-8. 2004.

[2] Kanthal, Swedish Patent #155,836; 1953.

[3] Mufit Akinc, M.K. Meyer, M. Kramer, A. Thom, J.J. Huebsch, B. Cook. "Boron-doped molybdenum silicides for structural applications". *Materials Science and Engineering A*, **261** (1999), 16-23.

[4] H. Nowotny, E. Dimakopoulou, H. Kudielka, *Mh. Chem.* **88** (1957) 180.

[5] D. M. Berczik, Method for enhancing the oxidation resistance of a molybdenum alloy, and a method of making a molybdenum alloy, United States Patent, Patent Number 5,595,616 (1997).

[6] J.H. Perepezko, D.M. Dimiduk, "Mo-Si-B Alloys: Developing a Revolutionary Turbine-Engine Material", *MRS Bulletin*, (2003).

[7] J.H. Schneibel, C.T. Liu, D.S. Easton, C.A. Carmichael. "Microstructure and mechanical properties of Mo–Mo_3Si–Mo_5SiB_2 silicides", *Materials Science and Engineering A*, **261** (1999), 78-83.

[8] J.H. Schneibel, M.J. Kramer, O. Unal, Richard Wright. "Processing and mechanical properties of a molybdenum silicide with the composition Mo-12Si-8.5B (at.%)", *Intermetallics* **9** (2001), 25-31.

[9] H. Choe, J.H. Schneibel, R.O. Ritchie, "On the Fracture and Fatigue Properties of Mo-Mo_3Si-Mo_5SiB_2 Refractory Intermetallic Alloys at Ambient to Elevated Temperatures (25°C to 1300°C)", *Metall. and Mat. Trans*. **34A** (2003), 225-39.

[10] P. Jéhanno, M. Heilmaier, H. Kestler, "Characterization of an industrially processed Mo-based silicide alloy", *Intermetallics* **12** (2004), 1005-9.

[11] P. Jéhanno, M. Heilmaier, H. Kestler, M. Boning, A. Venskutonis, B. Bewlay, M. Jackson, "Assessment of a powder processing route for refractory metal silicide alloys", *Metall. and Mat. Trans.* **36A** (2005), 515-523.

[12] L.E. Olds, G.W.P. Rengstorff, "Effect of Oxygen, Nitrogen, and Carbon on the Ductility of Cast Molybdenum", *Journal of Metals*, February 1956, 150-55.

[13] L.E. Olds, G.W.P. Rengstorff, "Effect of Small Amounts of Alloying Elements on the Ductility of Cast Molybdenum", *Journal of Metals*, April 1957, 468-71.

[14] S. Suzuki, H. Matsui, H. Kimura, "The Effect of Heat Treatment on the Grain Boundary Fracture of Recrystallized Molybdenum", *Materials Science and Engineering* **47** (1981), 209-16.

[15] A. Kumar, B. Eyre, "Grain Boundary Segregation and Intergranular Fracture in Molybdenum", *Proc. of the Royal Soc. of London, series A: Mathematical and Physical Sciences* **370** (1980), 431-58.

[16] J. Schneibel, R. Ritchie, J. Kruzic, P. Tortorelli, "Optimization of Mo-Si-B Intermetallic Alloys", *Metallurgical and Materials Transactions* **36A** (2005), 525-531.

[17] D.M. Scruggs, Ductile molybdenum composition containing a spinel dispersion, US Patent No. 3,320,036 (1963).

[18] S R Agnew; T Leonhardt, "The low-temperature mechanical behavior of molybdenum-rhenium", *JOM* **55**, 10 (2003), 25-29.

[19] R. Mitra, A.K. Srivastava, N.E. Prasad, S. Kumari, "Microstructure and mechanical behaviour of reaction hot pressed multiphase Mo-Si-B and Mo-Si-B-Al intermetallic alloys", *Intermetallics* **14** (2006), 1461-71.

[20] M. Middlemas, J.K. Cochran, "A Nitride-Based Reaction for the Formation of a Three-Phase Molybdenum-Silicon-Boron Intermetallic Alloy", Masters Thesis, School of Materials Science and Engineering, Georgia Institute of Technology, 2005.

[21] A. Alur, N. Chollacoop, K.S. Kumar, "High temperature compressive behavior of Mo-Si-B alloys", *Acta Materialia* **52** (2004), 5571-87.

[22] P. Jain, A. Alur, K.S. Kumar, "High temperature compressive flow behavior of a Mo-Si-B solid solution alloy", *Scripta Materialia* **54** (2006), 13-17.

[23] ASTM standard C1161–02c, "Standard Test Method for Flexural Strength of Advanced Ceramics at Ambient Temperature", ASTM International, revised 2002.

[24] MatWeb Online Material Data Sheet. © 2006 Automation Creations, Inc., http://www.matweb.com/search/SpecificMaterial.asp?bassnum=AMEMo01, 3/10/07.

[25] W.D. Kingery, H.K. Bowen, D.R. Uhlmann, *Introduction to Ceramics, 2nd Edition*, Wiley-Interscience, New York, 1976.

[26] K. Yanagihara, T. Manyama, K. Nagata, *Journal of the Institute of Metals* **34** (1993), 1200.